

---

# DISCO: Efficient Diffusion Solver for Large-Scale Combinatorial Optimization Problems

---

**Kexiong Yu**

National University of Defense Technology  
yukexiong18@nudt.edu.cn

**Hang Zhao**

National University of Defense Technology  
alex.hang.zhao@gmail.com

**Yuhang Huang**

National University of Defense Technology  
huangai@nudt.edu.cn

**Renjiao Yi**

National University of Defense Technology  
yirenjiao@nudt.edu.cn

**Kai Xu\***

National University of Defense Technology  
kevin.kai.xu@gmail.com

**Chenyang Zhu\***

National University of Defense Technology  
zhuchenyang07@nudt.edu.cn

## Abstract

Combinatorial Optimization (CO) problems are fundamentally crucial in numerous practical applications across diverse industries, characterized by entailing enormous solution space and demanding time-sensitive response. Despite significant advancements made by recent neural solvers, their limited expressiveness does not conform well to the multi-modal nature of CO landscapes. While some research has pivoted towards diffusion models, they require simulating a Markov chain with many steps to produce a sample, which is time-consuming and does not meet the efficiency requirement of real applications, especially at scale. We propose **DISCO**, an efficient **D**iffusion **S**olver for **C**ombinatorial **O**ptimization problems that excels in both solution quality and inference speed. DISCO’s efficacy is two-pronged: Firstly, it achieves rapid denoising of solutions through an analytically solvable form, allowing for direct sampling from the solution space with very few reverse-time steps, thereby drastically reducing inference time. Secondly, DISCO enhances solution quality by restricting the sampling space to a more constrained, meaningful domain guided by solution residues, while still preserving the inherent multi-modality of the output probabilistic distributions. DISCO achieves state-of-the-art results on very large Traveling Salesman Problems with 10000 nodes and challenging Maximal Independent Set benchmarks, with its per-instance denoising time up to 44.8 times faster. Through further combining a divide-and-conquer strategy, DISCO can be generalized to solve arbitrary-scale problem instances off the shelf, even outperforming models trained specifically on corresponding scales.

## 1 Introduction

Combinatorial Optimization (CO) is a fundamental field in both computer science and operations research, encompassing the search for an optimal solution from a finite set of entities. These challenges are widespread in various real-world applications across diverse industries, spanning logistics [57; 63], production scheduling [92; 95], and resource allocation [98; 100]. A distinctive characteristic of CO problems is the exponential expansion of their solution space as the problem scale increases. This exponential growth is particularly pronounced in the case of NP-complete (NPC)

---

\*Corresponding author

problems [27], representing the most formidable challenges within NP and posing a formidable obstacle to precisely finding an optimal solution within a polynomial time frame.

In recent years, deep learning algorithms have showcased remarkable capabilities in predicting CO solutions [15; 48]. However, these learning-based neural solvers are susceptible to being misled by the multi-modality inherent in CO problems [47], wherein the learning agent is required to identify a set of optimal solutions. This multi-modality complicates the learning process, hindering efficient convergence to desired solutions, particularly when confronted with large-scale instances [13; 89]. Diffusion probabilistic models [35; 69; 79] have demonstrated robust capabilities in various generation tasks. Of particular interest, Chi et al. [14] and Huang et al. [41] have employed diffusion methods for decision model construction, showcasing their inherent advantages in addressing multi-modal problems. This serves as inspiration for us to explore the application of diffusion models to CO problems, which similarly exhibit multi-modal characteristics.

We are not the first to apply diffusion models to CO problems. Graikos et al. [32] tackle Euclidean Traveling Salesman problems (TSP) by converting each instance into a low-resolution greyscale image and then utilizing a Convolutional Neural Network (CNN) [56] for denoising the solution. Sun and Yang [80] attempt to address this limitation by incorporating Graph Neural Networks (GNNs) [31] to explicit model problem structures. Although these approaches show improved performance, they require simulating a Markov chain with many steps for generation, which significantly incurs time overhead. This limitation inevitably hampers their practicality for time-sensitive real-world applications [28; 91], especially when dealing with large-scale instances.

We contend that the potential of diffusion models in addressing CO problems has yet to be fully discovered. We propose **DISCO**, an efficient **D**iffusion **S**olver for **C**ombinatorial **O**ptimization problems. DISCO obtains rapidly generating high-quality solutions with very few denoising steps and enhances solution quality by restricting the sampling space to a more constrained, meaningful domain guided by solution residues. DISCO achieves state-of-the-art results on large-scale TSP-10000 instances and challenging Maximal Independent Set (MIS) benchmarks, with its per-instance denoising time up to 44.8 times faster. Through further combining a divide-and-conquer strategy, DISCO can be generalized to solve arbitrary-scale problem instances off the shelf, even outperforming models trained specifically on corresponding scales.

## 2 Related Work

**Combinatorial Optimization** Combinatorial optimization (CO) problems have garnered considerable attention over the years due to their extensive applicability across diverse domains such as logistics [4; 52], production scheduling [92; 95], and resource allocation [98; 100]. However, the exponential growth of the solution space, as the problem scale escalates for these NPC problems [27], poses a formidable challenge for finding an optimal solution within a polynomial time frame. Traditional solvers for CO problems can be classified into exact algorithms, approximation algorithms, and heuristic methods. Exact algorithms [55; 74], such as dynamic programming [17] and cutting-plane methods [88], aim to exactly find the optimal solution for each test instance. However, they only suit small to medium-sized problems due to the inherent heavy computational complexity. Approximation [37; 84] and heuristic [29; 67] methods, on the other hand, are used when the problem scale is large or time constraints exist for finding solutions. These methods can find solutions within an acceptable time cost. However, they typically heavily rely on expert knowledge [34; 83] and cannot guarantee the high quality of the final discoveries.

**Learning for Combinatorial Optimization** With the blossoming of deep learning mechanisms that do not heavily rely on expert knowledge and can be easily adapted to various automated searching processes, researchers have widely explored neural solvers for CO problems. These approaches encompass both supervised learning (SL) [80; 86] and reinforcement learning (RL) [68; 82]. From a practical perspective, the choice between SL and RL depends on the availability of problem data. For online operation problems [8; 76], the input data is progressively revealed, and decisions must be made immediately upon data arrival. Such problems require algorithms to make decisions without fully understanding the problem, typically modeled as Markov Decision processes and solved through trial-and-error methods using RL [97; 99]. Conversely, for offline problems [66; 70], all input data and all constraints are fully provided before solving the problems. The decision-makers can fully utilize all relevant information for comprehensive analysis and iteratively improve solution quality. Providing an initial solution by SL and further refining it by decoding strategies [19; 26; 32; 52]

has become a common practice [22]. Most CO problems can be modeled as decision problems on graphs [59; 92; 93; 95]. Notably, the Traveling Salesman Problem (TSP) [7; 64] and the Maximum Independent Set (MIS) [12; 21] stand out as two foundations regarding edge and node decision problems. DISCO leverages anisotropic GNNs [10; 45] as the backbone to produce embeddings for both graph edges and nodes, adequately demonstrating its superiority on both TSP and MIS instances.

**Diffusion Probabilistic Model** Diffusion probabilistic models (DPMs) [35; 69; 79] are primarily utilized for high-quality generation and have exhibited robust capabilities in generating images [42; 94], audios [62], and videos [36; 87]. This impressive method was initially formulated by Sohl-Dickstein et al. [78] and further extended by Ho et al. [35] through the proposal of a general generation framework. Its principle involves simulating a forward process of gradually introducing noise, followed by training a reverse noise removal model to generate data. These models can further adjust the conditional variables [23] during the reverse process to generate data samples that satisfy specific attributes or conditions. In comparison to other generative models such as Generative Adversarial Networks (GANs) [30; 72], diffusion models demonstrate higher stability during training. This is attributed to their avoidance of adversarial training and they gradually approach the true distribution of the data by learning to remove noise.

**Diffusion for Combinatorial Optimization** In addition to stable and high-quality generation, DPMs have exhibited a promising prospect for generating a wide variety of distributions [35; 41]. This multi-modal property particularly benefits CO problem solving, where multiple optimal solutions may exist and confront the limited expressiveness of previous neural solvers [33; 47; 58]. Some attempts have been made. Graikos et al. [32] convert TSP instances into low-resolution greyscale images encoded by CNN while Sun and Yang [80] incorporate GNN [31] for problem representation. These efforts mainly focus on feature extraction and overlook the slow reverse process of diffusion models, which significantly hampers their practicality for time-sensitive real-world applications [28; 91], particularly at large scales. DISCO differentiates itself by developing a specialized diffusion process tailored for CO, optimizing both forward and reverse processes. Specifically, DISCO employs an analytical denoising process [40] to quickly produce high-quality solutions with very few denoising steps, while dramatically reducing solution space associated with NPC problems by introducing solution residues [60]. This enhanced efficiency on both inference speed and solution quality further amplifies DISCO’s generalization advantages on the CO challenge of arbitrary scales.

### 3 Preliminary

Combinatorial optimization can generically be framed as the task of finding a valid solution  $\mathbf{X}_s$  from a discrete solution space  $\mathcal{X}_s = \{0, 1\}^N$  for a given instance  $s$ , while minimizing the task-specific cost function  $\text{cost}(\mathbf{X}_s)$  [70]. The optimal solution  $\mathbf{X}_s^*$  is defined as:

$$\underset{\mathbf{X}_s \in \mathcal{X}_s}{\text{argmin}} \text{cost}(\mathbf{X}_s). \quad (1)$$

Taking TSP instances as an example,  $N$  represents the edge number,  $X_i \in \mathbf{X}_s$  indicates whether the  $i$ -th edge is selected, and  $\text{cost}_s(\mathbf{X})$  means the tour length of  $\mathbf{X}$ . Parameterized solvers, denoted as  $p(\cdot|s)$ , are trained to predict the probability distribution over each problem variable. Either supervised learning [80; 86] or reinforcement learning [4; 52] mechanisms have been extensively explored.

While previous neural CO solvers have shown promising results, they usually suffer from the expressiveness limitation when confronted with multiple optimal solutions for the same graph [33; 47]. Thanks to recent advances in generative models, DPMs have exhibited promising prospects for generating a wide variety of distributions [35; 41] suitable for CO solving.

DPMs view the input-to-noise process as a parameterized Markov chain that gradually adds noise to the original data  $\mathbf{x}_0$  until the signal is completely corrupted, this forward process is first formulated by Sohl-Dickstein et al. [78] with definition:

$$q(\mathbf{x}_t | \mathbf{x}_0) = \mathcal{N}(\mathbf{x}_t; \alpha_t \mathbf{x}_0, \beta_t^2 \mathbf{I}), \quad (2)$$

where  $\alpha_t$  and  $\beta_t$  are the differentiable functions of time  $t$  with bounded derivatives,  $\mathbf{x}_t$  is noisy data, and  $\mathbf{I}$  is the identity matrix. Kingma et al. [49] give proof that this Markov chain can be represented by the following stochastic differential equation:

$$d\mathbf{x}_t = h_t \mathbf{x}_t dt + g(t) d\mathbf{w}_t, \quad \mathbf{x}_0 \sim q(\mathbf{x}_0), \quad (3)$$

where  $h_t = \frac{d \log \alpha_t}{dt}$ ,  $g_t^2 = \frac{d\beta_t^2}{dt} - 2h_t \beta_t^2$ , and  $\mathbf{w}_t$  denotes the standard Wiener process [24].

## 4 Method

We introduce our analytical denoising process to generate high-quality solutions with very few reverse-time steps in Sec. 4.1. By introducing solution residues, as clarified in Sec. 4.2, we restrict the sampling space to a more constrained, meaningful domain, ensuring solution effectiveness while preserving diversity. In Sec. 4.3, we further generalize DISCO to solve arbitrary-scale CO problems combining with a multi-modality inspired divide-and-conquer strategy.

### 4.1 Analytically Solvable Denoising Process

Given problem instance  $s$ , parameterized DPM  $p(\cdot|s)$  generates conditionally independent probability distribution  $\mathbf{x}_0$  for each problem variable, also known as heatmap scores [26; 80]. Subsequently, task-specific decoding processes [19; 52] are employed to transform predicted  $\mathbf{x}_0$  into discrete solution  $\mathbf{X}_s$ . Typically, DPMs employ numerical integration during the reverse process, requiring multiple steps of accumulation and solving. This process incurs significant time overhead. For example, DDPM [35] usually takes 900 ~ 1000 sampling steps for meaningful image generation. The slow solving speed significantly limits the practical application of diffusion solvers for real-world CO problems, particularly considering many time-sensitive demands, such as on-call routing [28] and on-demand hailing service [91], not to mention the large-scale operation challenges.

To avoid time-consuming numerical integration and generate high-quality solutions with fewer steps, we substitute the numerical integration process with an analytically solvable form. Inspired by decoupled diffusion models (DDMs) [40], the original solution-to-noise mapping can be decoupled into solution-to-zero and zero-to-noise mapping:

$$\mathbf{x}_t = \mathbf{x}_0 + \int_0^t \mathbf{f}_t dt + \int_0^t d\mathbf{w}_t, \quad \mathbf{x}_0 \sim q(\mathbf{x}_0), \quad (4)$$

where  $\mathbf{x}_0 = \mathbf{X}_s$  denotes the high-quality solution label,  $\mathbf{x}_t$  is the noisy solution, and  $\mathbf{f}_t$  represents the analytic attenuation function. In the formulation,  $\mathbf{x}_0 + \int_0^t \mathbf{f}_t dt$  describes the solution attenuation and  $\int_0^t d\mathbf{w}_t$  describes the noise accumulation respectively. Decoupling the original solution-to-noise mapping into two relatively simpler processes improves the effectiveness of diffusion model training.

More importantly, since  $\mathbf{f}_t$  can be designed analytically, the efficiency of the reversed process can be improved by much fewer evaluation steps, e.g., inference with 1 or 2 steps. Based on Eq. 4, the transition probability from  $\mathbf{x}_0$  to  $\mathbf{x}_t$  can be defined as:

$$q(\mathbf{x}_t | \mathbf{x}_0) = \mathcal{N}(\mathbf{x}_t; \mathbf{x}_0 + \int_0^t \mathbf{f}_t dt, t\mathbf{I}). \quad (5)$$

For a reversed process, the sampling formula for  $\mathbf{x}_0$  is based on the analytic function  $\mathbf{f}_t$  that models the solution to zero transition process. We employ continuous-time Markov chain with the smallest time step  $\Delta t \rightarrow 0^+$  and use conditional distribution  $q(\mathbf{x}_{t-\Delta t} | \mathbf{x}_t, \mathbf{x}_0)$  to approximate  $q(\mathbf{x}_{t-\Delta t} | \mathbf{x}_t)$ , which is formulated by:

$$q(\mathbf{x}_{t-\Delta t} | \mathbf{x}_t, \mathbf{x}_0) \propto \exp\left\{-\frac{(\mathbf{x}_{t-\Delta t} - \tilde{\mathbf{u}})^2}{2\tilde{\sigma}^2\mathbf{I}}\right\}, \quad (6)$$

$$\tilde{\mathbf{u}} = \mathbf{x}_t - \int_{t-\Delta t}^t \mathbf{f}_t dt - \frac{\Delta t}{\sqrt{t}}\boldsymbol{\epsilon}, \quad \tilde{\sigma}^2 = \frac{\Delta t(t - \Delta t)}{t},$$

where  $\boldsymbol{\epsilon} \sim \mathcal{N}(\mathbf{0}, \mathbf{I})$ . Since  $\mathbf{f}_t$  has an analytic form, we can avoid the numerical integration-based denoising and instead directly sample heatmap  $\mathbf{x}_0$  with an arbitrary step size, which significantly reduces the inference time.

### 4.2 Residue-Constrained Solution Generation

The NPC solution space of CO problems exponentially grows with problem scales. The reverse generation covering such an enormous space is inefficient since many samples do even not adhere to problem constraints, as depicted in Fig. 1 (a). We propose to restrict the sampling space from the entire NPC space to a more constrained, meaningful domain while still preserving the multi-modality of the output probabilistic distributions. We achieve this by introducing solution residues [60] to prioritize certainty besides noises to emphasize diversity, as shown in Fig. 1 (b). The reversed process starts from both noise and an exceedingly economical degraded solution, confining the generated samples

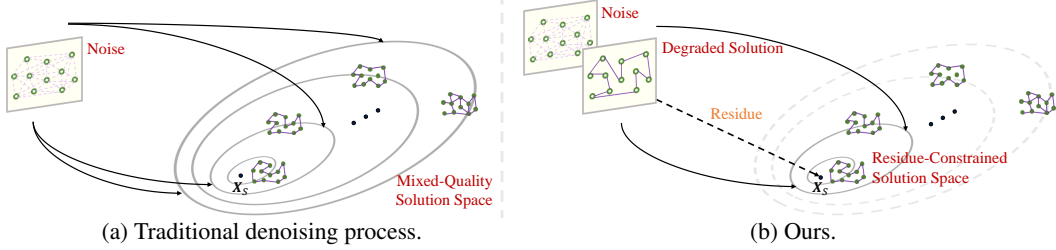


Figure 1: (a) The output of traditional diffusion processes spans the entire mixed-quality solution space, i.e., a significant proportion of the generations do not satisfy problem constraints besides high-quality heatmaps. (b) DISCO constrains the generations close to the high-quality label  $\mathbf{X}_s$  by introducing residues, resulting in a smaller but more meaningful solution space, while still preserving the multi-modality of the output distributions.

close to the high-quality input data. Driving a high-quality solution from a degraded or heuristic one has been verified as effective and is widely adopted in solving various CO problems [95; 100].

We denote  $\mathbf{X}_d$  a readily obtainable degraded solution that satisfies problem constraints and solution residues  $\mathbf{x}_{res} = \mathbf{X}_d - \mathbf{x}_0$ . Take TSP as an example,  $\mathbf{X}_d$  can be obtained by connecting vertices in the graph in a sequential order to form a tour. The forward process can be defined as:

$$\mathbf{x}_t = \mathbf{x}_0 + \int_0^t \mathbf{x}_{res} dt + \sqrt{t}\boldsymbol{\epsilon}, \quad \boldsymbol{\epsilon} \sim \mathcal{N}(\boldsymbol{\epsilon}; \mathbf{0}, \mathbf{I}). \quad (7)$$

Different from the original decoupled forward process, the first term of Eq. 7,  $\mathbf{x}_0 + \int_0^t \mathbf{x}_{res} dt$  represents the solution to degradation rather than solution to zero process. Intuitively, the former is much easier to learn since it only needs to predict the residue. Similar to Eq. 6, the transition probability of the reversed process is defined as:

$$q(\mathbf{x}_{t-\Delta t} | \mathbf{x}_t, \mathbf{x}_0) \propto \exp \left\{ -\frac{(\mathbf{x}_{t-\Delta t} - \mathbf{u})^2}{2\sigma^2 \mathbf{I}} \right\}, \quad (8)$$

$$\mathbf{u} = \mathbf{x}_t - \int_{t-\Delta t}^t \mathbf{x}_{res} dt - \Delta t \boldsymbol{\epsilon} / \sqrt{t}, \quad \sigma^2 = \Delta t(t - \Delta t) / t.$$

The residue prioritizes certainty while the noise emphasizes diversity, so that the solution space for sampling is effectively constrained. We also provide theoretical analysis about the equivalence between DISCO and DDM in App. A, supporting the effectiveness of our method.

**Training** We adopt anisotropic GNNs [10; 45] as the network architecture of DISCO. Unlike typical GNNs such as GCN [50] or GAT [85] designed for node-only embedding, anisotropic GNNs produce embeddings for both nodes and edges, which are then fed into the diffusion model to generate heatmaps. Practically, we input the noisy solution  $\mathbf{x}_t$ , the nodes and edges of  $\mathbf{X}_d$ , and the time  $t$  into the anisotropic GNN with parameter  $\boldsymbol{\theta}$ , predicting the parameterized residue  $\mathbf{x}_{res}^\theta$  and noise  $\boldsymbol{\epsilon}^\theta$  simultaneously. Specific implementation details are provided in App. G.

We focus on offline CO problems. Therefore, we train DISCO in an efficient and stable supervised mechanism to discover common patterns from high-quality solutions available for each instance. This also helps circumvent the challenges associated with scaling up and the latency in the inference that arises from the sparse rewards and sample efficiency issues when learning in an RL framework [65; 89], especially at large scales. The training objective is defined as:

$$\min_{\boldsymbol{\theta}} \mathbb{E}_{q(\mathbf{X}_s)} \mathbb{E}_{q(\boldsymbol{\epsilon})} [\|\mathbf{x}_{res}^\theta - \mathbf{x}_{res}\|^2 + \|\boldsymbol{\epsilon}^\theta - \boldsymbol{\epsilon}\|^2]. \quad (9)$$

After the model has been trained, it can be applied to generate heatmaps for a virtually unlimited number of unseen graphs during deployment. These heatmaps are fed into decoding strategies like Greedy [32], Sample [52], 2-opt [19], MCTS [26], and so on, for achieving the final solution.

**Sampling** Eq. 7 shows the endpoint of the forward process is the mixture of the degraded solution and noise, therefore, we start from the mixture in the sampling process. Given a degraded solution  $\mathbf{X}_d$  and a noise  $\boldsymbol{\epsilon}$  sampled from the normal distribution, we set  $\mathbf{x}_1 = \mathbf{X}_d + \boldsymbol{\epsilon}$  ( $t = 1$ ). Sampling from  $\mathbf{x}_1$  instead of  $\boldsymbol{\epsilon}$  constrains the sample space from the entire noise domain into a smaller one, ensuring an effective solution. For a  $K$ -step sampling, we set the step size of each sampling to  $1/K$ . At each

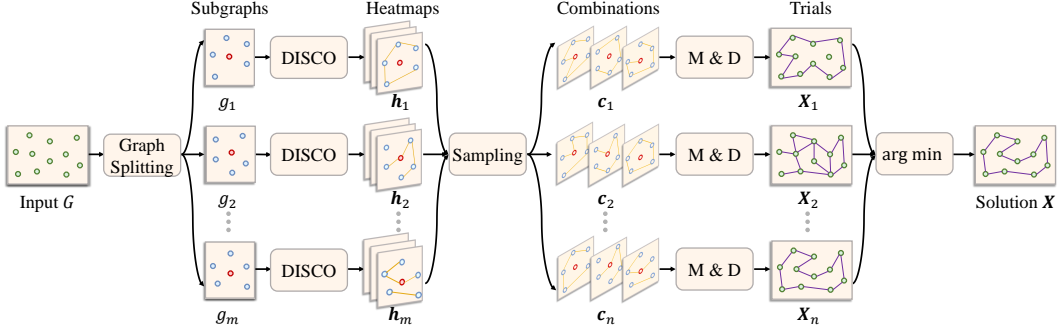


Figure 2: Our multi-modality inspired graph search method, illustrated using a TSP instance for simplicity. M & D denotes merging a combination of heatmaps  $\mathbf{c}$  to global heatmap  $\mathbf{H}$  and decoding a trial  $\mathbf{X}$  from  $\mathbf{H}$ .

sampling step, we utilize the anisotropic GNN to predict the estimated residue  $\mathbf{x}_{res}^\theta$  and noise  $\epsilon^\theta$ . In this way, we can solve the reversed process via Eq. 8 iteratively, obtaining the high-quality solution  $\mathbf{x}_0$  until  $t = 0$ . After we sample a probability distribution  $\mathbf{x}_0$  from  $p_\theta(s)$  for instance  $s$ , we adopt the same operation as [80] to obtain the normalized heatmap score  $\mathbf{h} = 0.5(\mathbf{x}_0 + 1)$ .

### 4.3 Multi-Modality Inspired Graph Search

Parameterized solvers trained on fixed scales often struggle to generalize well to test instances of different scales [26]. Training a model from scratch on the target scale or fine-tuning the model includes additional training time within the decision loop, making it impractical for real-world applications that demand an off-the-shelf response. We aim to further develop the generalization ability of DISCO to unseen-scale instances. With the efficiency advantage of DISCO in both inference speed and solution quality, along with the assistance of the SL approach in discovering common solution patterns, we can enhance this generalization ability through a divide-and-conquer strategy.

Specifically, we leverage a model  $p_\theta$  trained on a small scale to serve as a base and construct heatmaps for sub-problems  $\mathbf{g}$  decomposed from the original graph  $G$ , thereby smoothly generalize  $p_\theta$  to arbitrary scales. A detailed pipeline is provided in Fig. 2. We set each subgraph  $g \in \mathbf{g}$  with a fixed number of nodes for the decomposition. We adopt a vector  $\mathbf{o}_v$  recording the occurrence number of each node of  $G$  in all existing subgraphs. In each iteration, we choose the node with the index  $\text{argmin}(\mathbf{o}^v)$  as the cluster center and select the remaining nodes with the k-nearest neighbor rule [18], forming a subgraph  $g$ . This process continues until  $\min(\mathbf{o}^v)$  exceeds a certain threshold  $\omega$ . For each  $g \in \mathbf{g}$ , we resize it to a uniform size. Leveraging DISCO models  $p_\theta$  trained on a small problem scale, we can generate sub-heatmap score  $\mathbf{h}$  for  $g$ . The solution for the original graph  $G$  is obtained by merging all sub-heatmaps which jointly cover  $G$  at least  $\omega$  times. The merged global heatmap  $\mathbf{H}$  is calculated as follows:

$$\mathbf{H}_{ij} = \frac{1}{\mathbf{o}_{ij}} \times \sum_{l=1}^{|\mathbf{g}|} \phi(\mathbf{h}_l, i, j), \quad (10)$$

where  $\phi(\mathbf{h}_l, i, j)$  represents the heatmap value contributed by  $\mathbf{h}_l$  corresponding to index  $ij$  of  $\mathbf{H}$ , with  $\phi(\mathbf{h}_l, i, j) = 0$  if no correspondence. Subsequently, we decode the final solution  $\mathbf{X}$  from  $\mathbf{H}$ .

While the divide-and-conquer approach improves generalization performance, the preference of sub-heatmaps of selecting the locally shortest path may lead the final solution to get stuck in the sub-optimum. We further leverage the multi-modality of DISCO to enhance the solution diversity and avoid this sub-optimum dilemma. For each subgraph  $g \in \mathbf{g}$ , we repeatedly sample a set of heatmaps  $\mathcal{H}$  with  $q$  different noise  $\mathbf{x}_t$ . We randomly sample one heatmap  $\mathbf{h}$  from each  $\mathcal{H}$ , combining as a set  $\mathbf{c}$  with  $|\mathbf{c}| = |\mathbf{g}|$ , merging as a global heatmap  $\mathbf{H}$ , and decoding a solution trial  $\mathbf{X}$  from  $\mathbf{H}$ . This sample process is repeated  $n$  times, generating multiple trials as  $\mathcal{X}$ . We decide the final solution with

---

#### Algorithm 1 Multi-Modal Graph Search

---

**Input:** A graph problem  $G$  to be solved

**Process:**

- 1: Pre-train DISCO model  $p_\theta$  on a small scale
  - 2: Sample a set of subgraphs  $\mathbf{g}$  from  $G$
  - 3: **for**  $g \in \mathbf{g}$  **do**
  - 4: Sample heatmap set  $\mathcal{H}$  from  $p_\theta(g)$  with  $q$  different noise  $\mathbf{x}_t$
  - 5: **end for**
  - 6: Initialize trial set  $\mathcal{X} = \emptyset$
  - 7: **for**  $k = 1, 2, 3, \dots, n$  **do**
  - 8: Sample  $\mathbf{h}$  from each  $\mathcal{H}$  as combination  $\mathbf{c}_k$
  - 9: Merge  $\mathbf{c}_k$  as a global heatmap  $\mathbf{H}_k$
  - 10: Decode trial  $\mathbf{X}_k$  from  $\mathbf{H}_k$ , add it to  $\mathcal{X}$
  - 11: **end for**
  - 12: Select a final trial with  $\text{arg min}_{\mathbf{X} \in \mathcal{X}} \text{cost}(\mathbf{X})$
-

the minimum cost from  $\mathcal{X}$ , i.e.,  $\arg \min_{\mathbf{X} \in \mathcal{X}} \text{cost}(\mathbf{X})$ . Although there may be  $\exp_q(|\mathbf{g}|)$  possible combinations, we observe that the final performance asymptotically converges to the number of sampled trials, so we only need finite  $n$  samples. We also provide our detailed algorithm in Alg. 1.

## 5 Experiments

We provide extensive experimental results to demonstrate the superiority of DISCO. We begin by detailing the experimental settings in Sec. 5.1, followed by comparisons with state-of-the-art CO solvers on well-studied TSP problems in Sec. 5.2 to showcase DISCO’s performance. Subsequently, we conduct ablations on DISCO components in Sec. 5.3, verify its generalization ability to arbitrary problem scales in Sec. 5.4, and also assess its scalability in solving MIS problems in Sec. 5.5.

### 5.1 Experimental Settings

**Metrics** While DISCO is generically applicable to various NPC problems, we mainly conduct evaluations focused on the most representative TSP problems, as it is a common challenge in the machine learning community with well-studied competitors for demonstrating our method’s superiority. Given this, our evaluation metrics are the average length (Length) of predicted tours and the clock time (Time) required to generate solutions for all test instances, presented in seconds (s), minutes (m), or hours (h). We also report the performance gap (Gap), which is the average of the relative decrease in performance compared to a baseline method.

**Baselines** We extensively compare DISCO with various baselines, including exact solvers, heuristic solvers, and state-of-the-art learning methods. For exact solvers, our comparisons include Concorde [3] and Gurobi [61]. Regarding heuristic solvers, we evaluate against LKH-3 [34] and a simple Farthest Insertion principle [16]. In terms of learning-based methods, we compare with recent advances including AM [52], GCN [46], POMO [53], EAN [22], POMO + EAS [39], Att-GCN [26], DIMES [71], and a graph-based diffusion solver DIFUSCO [80].

We label the large-scale training instances using the LKH-3 heuristic solver [34] and we take the same test instances as [26; 80]. All evaluations are conducted on a single NVIDIA Tesla V100 GPU, paired by Intel(R) Xeon(R) Gold CPUs @ 2.50GHz, consistent with previous works [71; 80]. Some learning-based solvers struggle with large problem scales; for instance, Image Diffusion [32] only operates on a  $64 \times 64$  greyscale image. To ensure fairness, we compare them on small-scale instances. The results are provided in App. C, along with comparisons with Transformer [11], Sym-NCO [48], DPDP [65], and MDAM [90]. Our codes, trained models, and documentation are provided in the Supplementary Material and will be publicly released upon acceptance.

### 5.2 Comprehensive Comparisons

We compare DISCO to alternative NPC solvers across various problem scales, namely TSP-500, TSP-1000, and TSP-10000. Given that the approach of providing heatmaps by parameterized solvers and further transforming them into solutions by decoding strategies has become a common practice since 2018 [22], we report parameterized solvers’ performance combined with different decoding strategies including greedy [32], sampling [52], 2-opt [19], MCTS [26], and so on. We give a specific introduction to these decoding strategies in App. F. We particularly align the decoding settings of DISCO with DIFUSCO [80] to demonstrate its superiority as a diffusion solver. We follow Graikos et al. [32] and use the Greedy+2-opt decoding strategy as the default for all experiments. The sampling strategy is conducted by sampling 16 times for TSP-500 and TSP-1000, and 4 times for TSP-10000 [80]. The MCTS decoding strategy only samples one heatmap [71]. Unless otherwise specified, we set the denoising steps of DISCO to 2 to demonstrate its efficiency advantage. For DIFUSCO, we follow their settings and use 50 steps. We provide more evaluation details in App. G.

The comprehensive results are summarized in Tab. 1. We observe that both DIFUSCO and DISCO outperform the previous probabilistic solvers across all three settings, with DISCO dominating at larger TSP-10000 problem scales, even when combined with various decoding strategies. This underscores the importance of the diffusion choice, which inherently possesses multi-modal expressiveness that suits operation problems well. More importantly, DISCO exhibits an absolute advantage in inference speed compared to DIFUSCO, with its per-instance inference time achieving up to 44.8 times speedup, better satisfying many real-world applications that require time-sensitive responses. We also evaluate DISCO on real-world TSP scenarios from TSPLIB [73] in App. E. DISCO is the best performer in 28 out of 29 test cases while its inference speed surpasses all compared algorithms,

Table 1: Comparisons on large-scale TSP problems. AS, G, S, BS, and MCTS denotes Active Search [5], Greedy decoding, Sampling decoding, Beam Search [81], and Monte Carlo Tree Search [51], respectively. The symbol \* indicates the baseline for computing the performance gap. The symbol † denotes that the diffusion model samples once. The per-instance inference time for diffusion models DISCO/DIFUSCO is  $5.21 \times 10^{-2}/2.21(s)$  for TSP-500,  $1.23 \times 10^{-1}/5.51(s)$  for TSP-1000, and  $1.10/31.91(s)$  for TSP-10000 instances.

ALGORITHM	TYPE	TSP-500			TSP-1000			TSP-10000		
		LENGTH ↓	GAP ↓	TIME ↓	LENGTH ↓	GAP ↓	TIME ↓	LENGTH ↓	GAP ↓	TIME ↓
CONCORDE	EXACT	16.55*	—	37.66m	23.12*	—	6.65h	N/A	N/A	N/A
GUROBI	EXACT	16.55	0.00%	45.63h	N/A	N/A	N/A	N/A	N/A	N/A
LKH-3 (DEFAULT)	HEURISTICS	16.55	0.00%	46.28m	23.12	0.00%	2.57h	71.77*	—	8.8h
LKH-3 (LESS TRIALS)	HEURISTICS	16.55	0.00%	3.03m	23.12	0.00%	7.73m	71.79	—	51.27m
FARTHEST INSERTION	HEURISTICS	18.30	10.57%	0s	25.72	11.25%	0s	80.59	12.29%	6s
AM	RL+G	20.02	20.99%	1.51m	31.15	34.75%	3.18m	141.68	97.39%	5.99m
GCN	SL+G	29.72	79.61%	6.67m	48.62	110.29%	28.52m	N/A	N/A	N/A
POMO+EAS-EMB	RL+AS+G	19.24	16.25%	12.80h	N/A	N/A	N/A	N/A	N/A	N/A
POMO+EAS-TAB	RL+AS+G	24.54	48.22%	11.61h	49.56	114.36%	63.45h	N/A	N/A	N/A
DIMES	RL+G	18.93	14.38%	0.97m	26.58	14.97%	2.08m	86.44	20.44%	4.65m
DIMES	RL+AS+G	17.81	7.61%	2.10h	24.91	7.74%	4.49h	80.45	12.09%	3.07h
DIFUSCO	SL+G†+2-OPT	<b>16.80</b>	<b>1.49%</b>	3.65m	<b>23.56</b>	<b>1.90%</b>	12.06m	73.99	3.10%	35.38m
DISCO (Ours)	SL+G†+2-OPT	16.86	1.87%	0.25m	23.65	2.29%	1.12m	<b>73.85</b>	<b>2.90%</b>	25.12m
EAN	RL+S+2-OPT	23.75	43.57%	57.76m	47.73	106.46%	5.39h	N/A	N/A	N/A
AM	RL+BS	19.53	18.03%	21.99m	29.90	29.23%	1.64h	129.40	80.28%	1.81h
GCN	SL+BS	30.37	83.55%	38.02m	51.26	121.73%	51.67m	N/A	N/A	N/A
DIMES	RL+S	18.84	13.84%	1.06m	26.36	14.01%	2.38m	85.75	19.48%	4.80m
DIMES	RL+AS+S	17.80	7.55%	2.11h	24.89	7.70%	4.53h	80.42	12.05%	3.12h
DIFUSCO	SL+S+2-OPT	<b>16.65</b>	<b>0.57%</b>	11.46m	<b>23.45</b>	<b>1.43%</b>	48.09m	73.89	2.95%	6.72h
DISCO (Ours)	SL+S+2-OPT	16.73	1.09%	3.88m	23.56	1.90%	9.62m	<b>73.81</b>	<b>2.84%</b>	1.60h
ATT-GCN	SL+MCTS	16.97	2.54%	2.20m	23.86	3.22%	4.10m	74.93	4.39%	21.49m
DIMES	RL+MCTS	16.87	1.93%	2.92m	23.73	2.64%	6.87m	74.63	3.98%	29.83m
DIMES	RL+AS+MCTS	16.84	1.76%	2.15h	23.69	2.46%	4.62h	74.06	3.19%	3.57h
DIFUSCO	SL+MCTS	<b>16.63</b>	<b>0.46%</b>	10.13m	<b>23.39</b>	<b>1.17%</b>	24.47m	73.62	2.58%	47.36m
DISCO (Ours)	SL+MCTS	<b>16.63</b>	<b>0.46%</b>	6.99m	23.42	1.30%	15.82m	<b>73.56</b>	<b>2.49%</b>	42.35m

further validating the practicality of our method. We also provide comparisons of DISCO with more recent learning-based methods which are only trainable on small-scale instances in App. C, with DISCO consistently maintaining its advantage on both inference speed and solution quality. To facilitate a better understanding of our approach, we provide visual comparisons of denoising results in App. D. These include the evolution of generated heatmaps throughout the denoising process and the correlation between the final solution quality and the total number of diffusion steps.

### 5.3 Ablations on DISCO Components

We conduct ablation experiments on two key modules of DISCO: the analytical denoising process and residue constraints. The results are summarized in Tab. 2. We can observe that for the version without the analytical denoising, which can also be regarded as an equal implementation of DIFUSCO [80], its reverse process requires 50 steps to achieve satisfactory results; otherwise, the solution quality suffers. In contrast, with the analytical denoising process, we can obtain a satisfactory solution in just 2 steps, significantly improving inference speed. Moreover, the presence of residue constraints notably enhances the quality of generated heatmaps, as evident from a direct example in Fig. 3. The improvement in predicted heatmap quality naturally translates into higher solution quality, ultimately reflecting the efficacy of DISCO motivation.

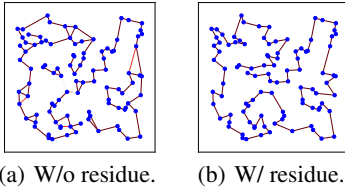


Figure 3: Akin to inner loops in a generated TSP heatmap (a), the denoised samples without residues span an enormous NPC space, leading to frequent failures in satisfying problem constraints as (b).

Table 2: Ablations on DISCO components. Step denotes the denoising step number. A and R represent the analytical diffusion process and residue constraints. Denoising with 1 step leads to near-zero variance, higher confidence, and potentially better performance.

	ALGORITHM	STEPS	TSP-1000			TSP-10000		
			LENGTH ↓	GAP(%) ↓	TIME ↓	LENGTH ↓	GAP(%) ↓	TIME ↓
GREEDY	W/o A&R	50	23.56	1.90%	12.06m	73.99	3.10%	35.38m
	W/o A&R	2	24.72	6.92%	1.37m	78.25	9.03%	27.01m
	W/o R	2	24.02	3.89%	1.33m	78.01	8.69%	20.60m
	DISCO	2	23.86	3.20%	1.37m	74.94	4.42%	26.18m
	DISCO	1	23.65	2.29%	1.12m	73.85	2.90%	25.12m
SAMPLING	W/o A&R	50	23.45	1.43%	48.09m	73.89	2.95%	6.72h
	W/o A&R	2	24.36	5.36%	21.35m	78.08	8.79%	1.78h
	W/o R	2	23.80	2.94%	25.82m	77.86	8.49%	1.87h
	DISCO	2	23.56	1.90%	9.62m	74.28	3.51%	1.67h
	DISCO	1	23.66	2.34%	7.22m	73.81	2.84%	1.60h

### 5.4 Multi-Modality Inspired Graph Search

Benefiting from DISCO’s verified advantage in both inference speed and solution quality, we can apply our multi-modality inspired graph search method to generalize a small-scale DISCO model  $p_\theta$  to solve the arbitrary scale problem instances off the shelf. We train base model  $p_\theta$  on TSP-100

Table 3: Results on multi-modality inspired graph search. O means merging all generated heatmap sets at once.

ALGORITHM	TYPE	TRIAL	TSP-500			TSP-1000			TSP-10000		
			LENGTH ↓	GAP ↓	TIME ↓	LENGTH ↓	GAP ↓	TIME ↓	LENGTH ↓	GAP ↓	TIME ↓
LKH-3 (DEFAULT)	HEURISTICS	-	16.55*	0.00%	46.28m	23.12*	0.00%	2.57h	71.77*	—	8.8h
ATT-GCN	SL+MCTS	1	16.97	2.54%	2.20m	23.86	3.22%	4.10m	74.93	4.39%	21.49m
DISCO (TSP-500)	SL+G†+2-OPT	1	<b>16.86</b>	<b>1.87%</b>	0.25m	23.97	3.68%	0.93m	76.03	5.94%	21.52m
DISCO (TSP-1000)	SL+G†+2-OPT	1	16.94	2.16%	0.23m	<b>23.65</b>	<b>2.29%</b>	1.12m	74.31	3.54%	22.65m
DISCO (TSP-10000)	SL+G†+2-OPT	1	17.28	4.25%	0.32m	24.19	4.63%	1.73m	<b>73.85</b>	<b>2.90%</b>	25.12m
DIFUSCO + O	SL+G†+2-OPT	1	17.20	3.70%	2.00h	24.00	3.81%	4.46h	74.33	3.57%	4.91h
DIFUSCO	SL+G†+2-OPT	50	16.96	2.48%	2.34h	23.78	2.85%	5.02h	74.35	3.60%	5.93h
DISCO + O	SL+G†+2-OPT	1	17.02	2.84%	3.33m	23.88	3.29%	9.45m	74.45	3.73%	36.43m
DISCO	SL+G†+2-OPT	50	<b>16.79</b>	<b>1.45%</b>	11.67m	<b>23.61</b>	<b>2.14%</b>	28.83m	<b>74.24</b>	<b>3.44%</b>	1.82h
DISCO	SL+G†+2-OPT	100	16.77	1.33%	18.26m	23.59	2.01%	42.33m	74.22	3.41%	3.76h
DISCO ( $\omega = 4$ )	SL+G†+2-OPT	50	16.78	1.39%	17.53m	23.61	2.12%	44.93m	74.23	3.43%	2.18h
DISCO	SL+MCTS	50	16.70	0.91%	18.81m	23.54	1.82%	42.19m	73.69	2.68%	2.10h

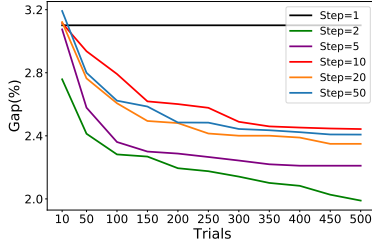


Figure 4: Asymptotic performance of multi-modal graph search with trial number.

Table 4: Results on MIS problems. TS denotes Tree Search [58].

METHOD	TYPE	SATLIB			ER-[700-800]		
		SIZE ↑	GAP ↓	TIME ↓	SIZE ↑	GAP ↓	TIME ↓
KAMIS	HEURISTICS	425.96*	—	37.58m	44.87*	—	52.13m
GUROBI	EXACT	425.95	0.00%	26.00m	41.38	7.78%	50.00m
DGL	SL+TS	N/A	N/A	N/A	37.26	16.96%	22.71m
INTEL	SL+TS	N/A	N/A	N/A	38.80	13.43%	20.00m
INTEL	SL+G	420.66	1.48%	23.05m	34.86	22.31%	6.06m
DIMES	RL+G	421.24	1.11%	24.17m	38.24	14.78%	6.12m
DIFUSCO	SL+G	424.50	0.34%	13.00m	38.83	12.40%	8.82m
DISCO (OURS)	SL+G	<b>424.58</b>	<b>0.32%</b>	10.32m	<b>40.30</b>	<b>10.17%</b>	9.00m
LwD	RL+S	422.22	0.88%	18.83m	41.17	8.25%	6.33m
DIMES	RL+S	423.28	0.63%	20.26m	42.06	6.26%	12.01m
DIFUSCO	SL+S	425.04	0.22%	26.09m	40.70	9.29%	17.33m
DISCO (OURS)	SL+S	<b>425.06</b>	<b>0.21%</b>	27.25m	<b>42.21</b>	<b>5.93%</b>	16.93m

instances and transfer it to TSP-500/1000/10000 instances. The results are summarized in Tab. 3. We can observe that when testing a trained model on a different problem scale, although DISCO generalizes decently, it performs less effectively compared to models trained on the equivalent scale. Meanwhile, our multi-modal graph search algorithm, combined with  $p_\theta$  trained only on TSP-100, exhibits better performance even when a substantial scale difference exists. With just 50 trials, it can even outperform models trained on the corresponding scale. Att-GCN [26] also adopts the decomposition mechanism for enhancing generalization. However, their parameterized solver lacks the ability to generate multiple trials, which causes the final solution may get stuck in the sub-optimum and be less effective than DISCO. Although DIFUSCO [80] also possesses the multi-modal property, its inference speed is prohibitively slow, requiring extensive test time to obtain satisfactory solutions.

While our graph search approach offers  $\exp_q(|g|)$  possibilities, the final performance asymptotically converges to the number of sampled trials, as confirmed in Fig. 4. The required sample number increases with solution variance, which is controlled by the number of denoising steps. We recommend 2-step denoising for better practice. We also compare our method with a variant that does not generate multiple trials, i.e., merging all generated heatmap sets  $\mathcal{H}$  at once, revealing that the multi-modality inspired search method generally outperforms this approach. This amplifies the importance of solution diversity for solving offline CO problems. DISCO’s performance can be further enhanced by trading off time costs through various means such as increasing sampled trials, augmenting the subgraph number  $|g|$  by controlling  $\omega$ , and re-decoding the merged heatmap combinations corresponding to the most promising trial with more sophisticated strategies like MCTS. These conclusions are also corroborated in Table 3.

## 5.5 Evaluations on Maximal Independent Set

Besides TSP instances, we also evaluate DISCO on commonly studied MIS problems, both of which are adequately representative of edge-based and node-based NPC problems. Evaluations are conducted on SATLIB [38] and Erdős-Rényi (ER) [25] graph sets, which exhibit challenge for recent learning-based solvers [1; 9; 58; 71]. The training instances are labeled by the KamIS heuristic solver [54] with test instances aligned with [71]. We adopt the same denoising steps and sample times as DIFUSCO [80] to distinguish model capabilities. Specific details of experimental settings and baselines can be found in App. B. We report the average size of the independent set (Size) in Tab. 4. DISCO exhibits an absolute performance advantage over all competitor algorithms.

## 6 Conclusion

We propose DISCO, an efficient diffusion solver for CO problems. DISCO obtains rapidly generating high-quality solutions with very few denoising steps and enhances solution quality by restricting the

sampling space by solution residues. DISCO achieves state-of-the-art results on large-scale TSP-10000 instances and challenging MIS benchmarks SATLIB and Erdős-Rényi, with its per-instance denoising time up to 44.8 times faster. Through further combining a divide-and-conquer strategy, DISCO can be generalized to solve arbitrary-scale problem instances off the shelf, even outperforming models trained specifically on those scales. This work focuses on solving offline problems with supervised approaches. Integrating DISCO to address online problems through trial and error is meaningful for future research. Employing an active learning approach that directly determines the best trial for the multi-modal graph search method, instead of sampling, would also be exciting.

## 7 Broader Impacts

Our proposed DISCO method is a general-purpose parameterized solver for CO problems. DISCO leverages diffusion technologies to address the multi-modal nature of CO problems effectively. DISCO optimizes both its forward and reverse processes more efficiently for solution generation, and significantly excels in both inference speed and solution quality. This improved efficiency further enhances DISCO’s capabilities to generalize to arbitrary-scale instances off the shelf. We believe that such efficient, learnable neural solvers for NPC problems will have a positive impact on a broad range of real-world applications [28; 91].

## References

- [1] S. Ahn, Y. Seo, and J. Shin. Learning what to defer for maximum independent sets. In International Conference on Machine Learning, 2020.
- [2] D. V. Andrade, M. G. Resende, and R. F. Werneck. Fast local search for the maximum independent set problem. Journal of Heuristics, 2012.
- [3] D. Applegate, R. Bixby, V. Chvatal, and W. Cook. Concorde tsp solver. <https://www.math.uwaterloo.ca/tsp/concorde/index.html>, 2006.
- [4] I. Bello, H. Pham, Q. V. Le, M. Norouzi, and S. Bengio. Neural combinatorial optimization with reinforcement learning. arXiv preprint arXiv:1611.09940, 2016.
- [5] I. Bello, H. Pham, Q. V. Le, M. Norouzi, and S. Bengio. Neural combinatorial optimization with reinforcement learning. In International Conference on Learning Representations, Workshop, 2017.
- [6] Y. Bengio, J. Louradour, R. Collobert, and J. Weston. Curriculum learning. In International Conference on Machine Learning, 2009.
- [7] J. Bi, Y. Ma, J. Wang, Z. Cao, J. Chen, Y. Sun, and Y. M. Chee. Learning generalizable models for vehicle routing problems via knowledge distillation. Advances in Neural Information Processing Systems, 2022.
- [8] A. Borodin and R. El-Yaniv. Online Computation and Competitive Analysis. Cambridge University Press, 2005.
- [9] M. Bötter, O. Kißig, M. Taraz, S. Cohen, K. Seidel, and T. Friedrich. What’s wrong with deep learning in tree search for combinatorial optimization. In International Conference on Learning Representations, 2022.
- [10] X. Bresson and T. Laurent. An experimental study of neural networks for variable graphs. 2018.
- [11] X. Bresson and T. Laurent. The transformer network for the traveling salesman problem. arXiv preprint arXiv:2103.03012, 2021.
- [12] L. Brusca, L. C. Quaedvlieg, S. Skoulakis, G. Chrysos, and V. Cevher. Maximum independent set: Self-training through dynamic programming. Advances in Neural Information Processing Systems, 2024.

- [13] X. Chen and Y. Tian. Learning to perform local rewriting for combinatorial optimization. Advances in Neural Information Processing Systems, 2019.
- [14] C. Chi, S. Feng, Y. Du, Z. Xu, E. Cousineau, B. Burchfiel, and S. Song. Diffusion policy: Visuomotor policy learning via action diffusion. In Robotics: Science and Systems, 2023.
- [15] J. Choo, Y.-D. Kwon, J. Kim, J. Jae, A. Hottung, K. Tierney, and Y. Gwon. Simulation-guided beam search for neural combinatorial optimization. Advances in Neural Information Processing Systems, 2022.
- [16] W. J. Cook, D. L. Applegate, R. E. Bixby, and V. Chvátal. The Traveling Salesman Problem: a Computational Study. Princeton University Press, 2011.
- [17] T. H. Cormen, C. E. Leiserson, R. L. Rivest, and C. Stein. Introduction to Algorithms. MIT press, 2022.
- [18] T. Cover and P. Hart. Nearest neighbor pattern classification. IEEE Transactions on Information Theory, 1967.
- [19] G. A. Croes. A method for solving traveling-salesman problems. Operations Research, 1958.
- [20] P. R. d O Costa, J. Rhuggenaath, Y. Zhang, and A. Akcay. Learning 2-opt heuristics for the traveling salesman problem via deep reinforcement learning. In Asian Conference on Machine Learning, 2020.
- [21] V.-A. Darvari, S. Hailes, and M. Musolesi. Solving graph-based public goods games with tree search and imitation learning. Advances in Neural Information Processing Systems, 2021.
- [22] M. Deudon, P. Cournut, A. Lacoste, Y. Adulyasak, and L.-M. Rousseau. Learning heuristics for the tsp by policy gradient. In Integration of Constraint Programming, Artificial Intelligence, and Operations Research, 2018.
- [23] P. Dhariwal and A. Nichol. Diffusion models beat gans on image synthesis. Advances in Neural Information Processing Systems, 2021.
- [24] A. Einstein et al. On the motion of small particles suspended in liquids at rest required by the molecular-kinetic theory of heat. Annalen Der Physik, 1905.
- [25] P. Erdős, A. Rényi, et al. On the evolution of random graphs. Publications of the Mathematical Institute of the Hungarian Academy of Sciences, 1960.
- [26] Z. Fu, K. Qiu, and H. Zha. Generalize a small pre-trained model to arbitrarily large TSP instances. In AAAI Conference on Artificial Intelligence, 2021.
- [27] M. R. Garey and D. S. Johnson. Computers and Intractability. Freeman San Francisco, 1979.
- [28] G. Ghiani, F. Guerriero, G. Laporte, and R. Musmanno. Real-time vehicle routing: Solution concepts, algorithms and parallel computing strategies. European Journal of Operational Research, 2003.
- [29] F. W. Glover and G. A. Kochenberger. Handbook of Metaheuristics. Springer Science & Business Media, 2006.
- [30] I. Goodfellow, J. Pouget-Abadie, M. Mirza, B. Xu, D. Warde-Farley, S. Ozair, A. Courville, and Y. Bengio. Generative adversarial nets. Advances in Neural Information Processing Systems, 2014.
- [31] M. Gori, G. Monfardini, and F. Scarselli. A new model for learning in graph domains. In International Joint Conference on Neural Networks, 2005.
- [32] A. Graikos, N. Malkin, N. Jovic, and D. Samaras. Diffusion models as plug-and-play priors. Advances in Neural Information Processing Systems, 2022.
- [33] J. Gu, J. Bradbury, C. Xiong, V. O. K. Li, and R. Socher. Non-autoregressive neural machine translation. In International Conference on Learning Representation, 2018.

- [34] K. Helsgaun. An extension of the lin-kernighan-helsgaun tsp solver for constrained traveling salesman and vehicle routing problems. Roskilde University, 2017.
- [35] J. Ho, A. Jain, and P. Abbeel. Denoising diffusion probabilistic models. In Advances in Neural Information Processing Systems, 2020.
- [36] J. Ho, T. Salimans, A. Gritsenko, W. Chan, M. Norouzi, and D. J. Fleet. Video diffusion models. Advances in Neural Information Processing Systems, 2022.
- [37] D. S. Hochba. Approximation algorithms for np-hard problems. ACM Sigact News, 1997.
- [38] H. H. Hoos and T. Stützle. Satlib: An online resource for research on sat. Sat, 2000.
- [39] A. Hottung, Y. Kwon, and K. Tierney. Efficient active search for combinatorial optimization problems. In International Conference on Learning Representations, 2022.
- [40] Y. Huang, Z. Qin, X. Liu, and K. Xu. Decoupled diffusion models with explicit transition probability. arXiv preprint arXiv:2306.13720, 2023.
- [41] Z. Huang, L. Liang, Z. Ling, X. Li, C. Gan, and H. Su. Reparameterized policy learning for multimodal trajectory optimization. In International Conference on Machine Learning, 2023.
- [42] Z. Huang, P. Zhou, S. Yan, and L. Lin. Scalelong: Towards more stable training of diffusion model via scaling network long skip connection. Advances in Neural Information Processing Systems, 2023.
- [43] B. Hudson, Q. Li, M. Malencia, and A. Prorok. Graph neural network guided local search for the traveling salesperson problem. In International Conference on Learning Representations, 2022.
- [44] E. T. Jaynes. Probability Theory: the Logic of Science. Cambridge University Press, 2003.
- [45] C. K. Joshi, Q. Cappart, L.-M. Rousseau, and T. Laurent. Learning the travelling salesperson problem requires rethinking generalization. Constraints, 2022.
- [46] C. K. Joshi, T. Laurent, and X. Bresson. An efficient graph convolutional network technique for the travelling salesman problem. arXiv preprint arXiv:1906.01227, 2019.
- [47] E. Khalil, H. Dai, Y. Zhang, B. Dilkina, and L. Song. Learning combinatorial optimization algorithms over graphs. Advances in Neural Information Processing Systems, 2017.
- [48] M. Kim, J. Park, and J. Park. Sym-nco: Leveraging symmetricity for neural combinatorial optimization. Advances in Neural Information Processing Systems, 2022.
- [49] D. Kingma, T. Salimans, B. Poole, and J. Ho. Variational diffusion models. Advances in Neural Information Processing Systems, 2021.
- [50] T. N. Kipf and M. Welling. Semi-supervised classification with graph convolutional networks. arXiv preprint arXiv:1609.02907, 2016.
- [51] L. Kocsis and C. Szepesvári. Bandit based monte-carlo planning. In European Conference on Machine Learning, pages 282–293. Springer, 2006.
- [52] W. Kool, H. van Hoof, and M. Welling. Attention, learn to solve routing problems! In International Conference on Learning Representations, 2019.
- [53] Y.-D. Kwon, J. Choo, B. Kim, I. Yoon, Y. Gwon, and S. Min. Pomo: Policy optimization with multiple optima for reinforcement learning. Advances in Neural Information Processing Systems, 2020.
- [54] S. Lamm, P. Sanders, C. Schulz, D. Strash, and R. F. Werneck. Finding near-optimal independent sets at scale. In Workshop on Algorithm Engineering and Experiments, 2016.
- [55] E. L. Lawler and D. E. Wood. Branch-and-bound methods: A survey. Operations Research, 1966.

- [56] Y. LeCun, L. Bottou, Y. Bengio, and P. Haffner. Gradient-based learning applied to document recognition. Proceedings of the IEEE, 1998.
- [57] Y. Li, J. Guo, R. Wang, and J. Yan. From distribution learning in training to gradient search in testing for combinatorial optimization. Advances in Neural Information Processing Systems, 2024.
- [58] Z. Li, Q. Chen, and V. Koltun. Combinatorial optimization with graph convolutional networks and guided tree search. Advances in Neural Information Processing Systems, 2018.
- [59] Z. Li and X. Si. Nsnet: A general neural probabilistic framework for satisfiability problems. Advances in Neural Information Processing Systems, 2022.
- [60] J. Liu, Q. Wang, H. Fan, Y. Wang, Y. Tang, and L. Qu. Residual denoising diffusion models. In Computer Vision and Pattern Recognition, 2024.
- [61] LLC Gurobi Optimization. Gurobi Optimizer Reference Manual, 2018.
- [62] S. Luo, C. Yan, C. Hu, and H. Zhao. Diff-foley: Synchronized video-to-audio synthesis with latent diffusion models. Advances in Neural Information Processing Systems, 2024.
- [63] Y. Ma, Z. Cao, and Y. M. Chee. Learning to search feasible and infeasible regions of routing problems with flexible neural k-opt. In Advances in Neural Information Processing Systems, 2023.
- [64] Y. Ma, Z. Cao, and Y. M. Chee. Learning to search feasible and infeasible regions of routing problems with flexible neural k-opt. Advances in Neural Information Processing Systems, 2024.
- [65] Y. Ma, J. Li, Z. Cao, W. Song, L. Zhang, Z. Chen, and J. Tang. Learning to iteratively solve routing problems with dual-aspect collaborative transformer. Advances in Neural Information Processing Systems, 2021.
- [66] S. Martello, D. Pisinger, and D. Vigo. The three-dimensional bin packing problem. Operations Research, 2000.
- [67] Z. Michalewicz and D. B. Fogel. How to Solve It: Modern Heuristics. Springer Science & Business Media, 2013.
- [68] V. Mnih, K. Kavukcuoglu, D. Silver, A. A. Rusu, J. Veness, M. G. Bellemare, A. Graves, M. Riedmiller, A. K. Fidjeland, G. Ostrovski, et al. Human-level control through deep reinforcement learning. Nature, 2015.
- [69] A. Q. Nichol and P. Dhariwal. Improved denoising diffusion probabilistic models. In International Conference on Machine Learning, 2021.
- [70] C. H. Papadimitriou and K. Steiglitz. Combinatorial Optimization: Algorithms and Complexity. Courier Corporation, 1998.
- [71] R. Qiu, Z. Sun, and Y. Yang. DIMES: A differentiable meta solver for combinatorial optimization problems. In Advances in Neural Information Processing Systems, 2022.
- [72] A. Radford, L. Metz, and S. Chintala. Unsupervised representation learning with deep convolutional generative adversarial networks. arXiv preprint arXiv:1511.06434, 2015.
- [73] G. Reinelt. Tsplib—a traveling salesman problem library. ORSA Journal on Computing, 1991.
- [74] A. Schrijver et al. Combinatorial Optimization: Polyhedra and Efficiency. Springer, 2003.
- [75] J. Schrittwieser, I. Antonoglou, T. Hubert, K. Simonyan, L. Sifre, S. Schmitt, A. Guez, E. Lockhart, D. Hassabis, T. Graepel, et al. Mastering atari, go, chess and shogi by planning with a learned model. Nature, 2020.
- [76] S. S. Seiden. On the online bin packing problem. Journal of the ACM, 2002.

- [77] D. Silver, A. Huang, C. J. Maddison, A. Guez, L. Sifre, G. Van Den Driessche, J. Schrittwieser, I. Antonoglou, V. Panneershelvam, M. Lanctot, et al. Mastering the game of go with deep neural networks and tree search. Nature, 2016.
- [78] J. Sohl-Dickstein, E. Weiss, N. Maheswaranathan, and S. Ganguli. Deep unsupervised learning using nonequilibrium thermodynamics. In International Conference on Machine Learning, 2015.
- [79] J. Song, C. Meng, and S. Ermon. Denoising diffusion implicit models. In International Conference on Learning Representations, 2021.
- [80] Z. Sun and Y. Yang. DIFUSCO: graph-based diffusion solvers for combinatorial optimization. In Advances in Neural Information Processing Systems, 2023.
- [81] I. Sutskever, O. Vinyals, and Q. V. Le. Sequence to sequence learning with neural networks. Advances in Neural Information Processing Systems, 2014.
- [82] R. S. Sutton and A. G. Barto. Reinforcement Learning: An Introduction. MIT Press, 2018.
- [83] É. D. Taillard and K. Helsgaun. Popmusic for the travelling salesman problem. European Journal of Operational Research, 2019.
- [84] V. V. Vazirani. Approximation Algorithms. Springer, 2001.
- [85] P. Velickovic, G. Cucurull, A. Casanova, A. Romero, P. Lio, Y. Bengio, et al. Graph attention networks. Stat, 2017.
- [86] O. Vinyals, M. Fortunato, and N. Jaitly. Pointer networks. Advances in Neural Information Processing Systems, 2015.
- [87] V. Voleti, A. Jolicoeur-Martineau, and C. Pal. Mcvd-masked conditional video diffusion for prediction, generation, and interpolation. Advances in Neural Information Processing Systems, 2022.
- [88] L. A. Wolsey and G. L. Nemhauser. Integer and Combinatorial Optimization. John Wiley & Sons, 2014.
- [89] Y. Wu, W. Song, Z. Cao, J. Zhang, and A. Lim. Learning improvement heuristics for solving routing problems. IEEE Transactions on Neural Networks and Learning Systems, 2021.
- [90] L. Xin, W. Song, Z. Cao, and J. Zhang. Multi-decoder attention model with embedding glimpse for solving vehicle routing problems. In AAAI Conference on Artificial Intelligence, 2021.
- [91] Z. Xu, Z. Li, Q. Guan, D. Zhang, Q. Li, J. Nan, C. Liu, W. Bian, and J. Ye. Large-scale order dispatch in on-demand ride-hailing platforms: A learning and planning approach. In ACM SIGKDD International Conference on Knowledge Discovery & Data Mining, 2018.
- [92] H. Ye, J. Wang, Z. Cao, H. Liang, and Y. Li. Deepaco: Neural-enhanced ant systems for combinatorial optimization. Advances in Neural Information Processing Systems, 2024.
- [93] E. Yolcu and B. Póczos. Learning local search heuristics for boolean satisfiability. Advances in Neural Information Processing Systems, 2019.
- [94] P. Yu, Y. Zhu, S. Xie, X. S. Ma, R. Gao, S.-C. Zhu, and Y. N. Wu. Learning energy-based prior model with diffusion-amortized mcmc. Advances in Neural Information Processing Systems, 2024.
- [95] C. Zhang, Z. Cao, W. Song, Y. Wu, and J. Zhang. Deep reinforcement learning guided improvement heuristic for job shop scheduling. In International Conference on Learning Representations, 2024.
- [96] Y. Zhang, S. Wang, G. Ji, et al. A comprehensive survey on particle swarm optimization algorithm and its applications. Mathematical Problems in Engineering, 2015.

- [97] H. Zhao, Z. Pan, Y. Yu, and K. Xu. Learning physically realizable skills for online packing of general 3D shapes. ACM Transactions on Graphics, 2023.
- [98] H. Zhao, Q. She, C. Zhu, Y. Yang, and K. Xu. Online 3D bin packing with constrained deep reinforcement learning. In AAAI Conference on Artificial Intelligence, 2021.
- [99] H. Zhao, Y. Yu, and K. Xu. Learning efficient online 3D bin packing on packing configuration trees. In International Conference on Learning Representations, 2021.
- [100] H. Zhao, C. Zhu, X. Xu, H. Huang, and K. Xu. Learning practically feasible policies for online 3D bin packing. Science China Information Sciences, 2022.

## Appendix

### A Equivalence Analysis between DDM and DISCO

Real-world combinatorial optimization (CO) problems often require the rapid generation of high-quality solutions  $\mathbf{X}_s$  for problem instance  $s$ . Previous neural solvers have suffered from the expressiveness limitation when confronted with multiple optimal solutions for the same graph [33; 47; 58]. In contrast, diffusion probabilistic models (DPMs) [35] have shown promising prospects for generating a wide variety of distributions suitable for CO solving. The only bottleneck is the slow inference speed of DPMs. This is due to DPMs employing numerical integration during the reverse process, requiring multiple steps of accumulation and solving and significantly incurring time overhead.

Inspired by decoupled diffusion models (DDMs) [40], we substitute the time-consuming numerical integration process with an analytically solvable form. The original solution-to-noise mapping can be decoupled into solution-to-zero and zero-to-noise mapping:

$$\mathbf{x}_t = \mathbf{x}_0 + \int_0^t \mathbf{f}_t dt + \int_0^t d\mathbf{w}_t, \quad \mathbf{x}_0 \sim q(\mathbf{x}_0), \quad (11)$$

where  $\mathbf{x}_0 + \int_0^t \mathbf{f}_t dt$  describes the solution attenuation and  $\int_0^t d\mathbf{w}_t$  describes the noise accumulation. Since  $\mathbf{f}_t$  can be designed analytically, the efficiency of the reversed process can be improved by much fewer evaluation steps, e.g., inference steps = 1 or 2. The distribution of  $\mathbf{x}_t$  conditioned on  $\mathbf{x}_0$  is defined as:

$$q(\mathbf{x}_t | \mathbf{x}_0) = \mathcal{N}(\mathbf{x}_t; \mathbf{x}_0 + \mathbf{F}_t, t\mathbf{I}), \quad (12)$$

where  $\mathbf{F}_t = \int_0^t \mathbf{f}_t dt$  and we sample  $\mathbf{x}_t$  by  $\mathbf{x}_t = \mathbf{x}_0 + \mathbf{F}_t + \sqrt{t}\epsilon$  with  $\epsilon \sim \mathcal{N}(\mathbf{0}, \mathbf{I})$ .

For a reverse time, the sampling formula for  $\mathbf{x}_0$  is based on the analytic attenuation function  $\mathbf{f}_t$  that models image to zero transition. We employ continuous-time Markov chain with the smallest time step  $\delta t \rightarrow 0^+$  and use conditional distribution  $q(\mathbf{x}_{t-\Delta t} | \mathbf{x}_t, \mathbf{x}_0)$  to approximate  $q(\mathbf{x}_{t-\Delta t} | \mathbf{x}_t, \mathbf{x}_0)$ .

$$q(\mathbf{x}_{t-\Delta t} | \mathbf{x}_t, \mathbf{x}_0) \propto \exp \left\{ -\frac{(\mathbf{x}_{t-\Delta t} - \tilde{\mathbf{u}})^2}{2\tilde{\sigma}^2\mathbf{I}} \right\}, \quad (13)$$

where  $\epsilon \sim \mathcal{N}(\mathbf{0}, \mathbf{I})$ ,  $\tilde{\mathbf{u}} = \mathbf{x}_t + \mathbf{F}_{t-\Delta t} - \mathbf{F}_t + \epsilon\Delta t/\sqrt{t}$ , and  $\tilde{\sigma}^2 = \Delta t(t - \Delta t)/t$ . Since  $\mathbf{f}_t$  has an analytic form, we can avoid the ordinary differential equation-based denoising and instead directly sample  $\mathbf{x}_0$  with an arbitrary step size, which significantly reduces the inference time.

Although the inference speed can benefit from the analytically solvable form, denoising methods still require inefficient sampling from the entire NPC solution space of CO problems, which typically grows exponentially with the number of problem scale  $N$ . We propose to constrain the sampling space into a smaller one by introducing residues [60] to DDM, which is our **DISCO** method, i.e., an efficient **D**iffusion **S**olver for **CO** problems. The reversed process starts from both noise and an exceedingly cost-effective degraded solution, confining the generation process in a smaller but more meaningful domain close to the high-quality labels. The residue prioritizes certainty while the noise emphasizes diversity, so that to ensure solution effectiveness while still maintaining their multi-modality property

Instead of the traditional forward process merely outputting noise, it is now a combination of noise  $\mathbf{x}_t$  and a degraded solution  $\mathbf{X}_d$  for generating residue constraints  $\mathbf{x}_{res} = \mathbf{X}_d - \mathbf{x}_0$ . The degraded solution  $\mathbf{X}_d$  is an exceedingly cost-effective path but satisfies problem constants. For example,  $0 - 1 - \dots - n - 0$ , connecting nodes in sequential order. Since DDM has already demonstrated its equivalence to previous diffusion processes defined by Equation 3 [40], we now provide proof of the equivalence between our method and DDM to demonstrate the effectiveness of DISCO in a theoretical aspect.

**Forward Process** The proposed forward formula considering residue is:

$$\mathbf{x}_t = \mathbf{x}_0 + \int_0^t \mathbf{x}_{res} dt + \sqrt{t}\epsilon. \quad (14)$$

Compared with the original forward formulation of DDM (Eq. 4), the proposed forward formulation utilizes a different function  $\mathbf{x}_{res}$  substituting the attenuation function  $\mathbf{f}_t$ , which means the two diffusion processes are equivalent.

**Reversed Process** In the reversed process, we need to parameterize two components:  $\mathbf{x}_{res}^\theta$  and  $\epsilon^\theta$ , which estimate the residue  $\mathbf{x}_{res}$  and the noise  $\epsilon$ , respectively. From Eq. 7, we have:

$$\mathbf{x}_0 = \mathbf{x}_t - \int_0^t \mathbf{x}_{res} dt - \sqrt{t}\epsilon. \quad (15)$$

Thus, the reverse process can be defined as:

$$p_\theta(\mathbf{x}_{t-\Delta t} | \mathbf{x}_t) := q(\mathbf{x}_{t-\Delta t} | \mathbf{x}_t, \mathbf{x}_0). \quad (16)$$

Applying Bayes' theorem [44], we obtain:

$$\begin{aligned} q(\mathbf{x}_{t-\Delta t} | \mathbf{x}_t, \mathbf{x}_0) &= \frac{q(\mathbf{x}_t | \mathbf{x}_{t-\Delta t})q(\mathbf{x}_{t-\Delta t} | \mathbf{x}_t)}{q(\mathbf{x}_t | \mathbf{x}_0)} \\ &= \frac{q(\mathbf{x}_t | \mathbf{x}_{t-\Delta t})\mathcal{N}(\mathbf{x}_{t-\Delta t}; \mathbf{x}_0 + \mathbf{H}_{t-\Delta t}, (t - \Delta t)\mathbf{I})}{\mathcal{N}(\mathbf{x}_t; \mathbf{x}_0 + \mathbf{F}_t, t\mathbf{I})}. \end{aligned} \quad (17)$$

Eq. 17 aligns with the reverse process in DDM, thus the reverse process formula is:

$$q(\mathbf{x}_{t-\Delta t} | \mathbf{x}_t, \mathbf{x}_0) \propto \exp\left(-\frac{(\mathbf{x}_{t-\Delta t} - \mathbf{u})^2}{2\sigma^2\mathbf{I}}\right), \quad (18)$$

where  $\tilde{\mathbf{u}} = \mathbf{x}_t - \int_{t-\Delta t}^t h_t dt - \frac{\Delta t}{\sqrt{t}}\epsilon$ ,  $\tilde{\sigma}^2 = \frac{\Delta t(t-\Delta t)}{t}$ , equivalent to the reverse formula of DDM.

## B Maximal Independent Set

Besides the TSP problem, we also evaluate DISCO on commonly studied MIS problems, both of which are adequately representative of edge-based and node-based NPC problems. We give specific details of experimental settings in this section.

**Datasets** We conduct evaluations on SATLIB [38] and Erdős-Rényi (ER) [25] graph sets, which exhibit challenge for recent learning-based solvers [1; 9; 58; 71]. The training instances of labeled by the KaMIS heuristic solver [54]. The split of test instances on SAT datasets and the random-generated ER test graphs are taken from [71].

**Metrics** We compare the performance of different probabilistic solvers by the average size (Size) of the predicted maximal independent set for each test instance; larger sizes indicate better performance. We also use the same Gap and Time definitions as in the TSP case. We adopt the same denoising steps and sample times as DIFUSCO [80] to distinguish model capabilities. Specifically, we use 50 steps for denoising heatmap and generate 4 times for sampling strategies. Following the principle of efficiency, we random sample a set of nodes from the original graph with a probability of 50% to obtain the degraded solution.

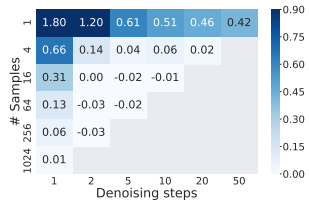
**Baselines** We compare DISCO with 7 other MIS solvers on the same test sets, including two traditional OR methods and five learning-based approaches. For the traditional methods, we use Gurobi and KaMIS [54] as baselines. For the learning-based methods, we compare with LwD [1], Intel [58], DGL [9], DIMES [71], and DIFUSCO [80].

## C Comparisons on Small-Scale TSP Instances

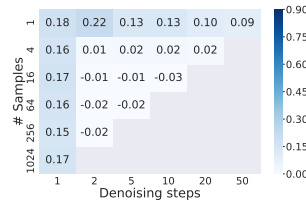
Some learning-based solvers struggle with large problem scales, we compare them on small-scale instances to ensure fairness. Specifically, we compare with learning-based methods Image Diffusion [32], Transformer [11], Sym-NCO [48], DPDP [65], and MDAM [90]. Along with the learning-based methods works on large scales including AM [52], GCN [46], POMO [53], EAN [22], POMO + EAS [39], Att-GCN [26], DIMES [71], and DIFUSCO [80]. We also make comparisons with traditional operation methods including Concorde [3] and Gurobi [61], LKH-3 [34], 2-OPT [19], and Farthest Insertion [16]. We label the training instances using the Concorde solver for TSP-50/100 and we take the same test instances as [45; 52]. The comprehensive results are summarized in Tab. 5, with DISCO consistently maintaining its advantage on both inference speed and solution quality. We visualize the performance and time-cost of DISCO on TSP-50 in Fig. 5, along with performance comparisons with previous diffusion solver DIFUSCO [80]. Corresponding denoising processes are provided in Fig. 6.

Table 5: Comparisons on TSP-50 and TSP-100. The symbol \* denotes the baseline for computing the performance gap. The symbol † indicates that the diffusion model samples once.

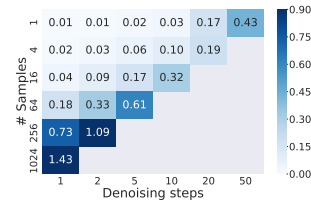
ALGORITHM	TYPE	TSP-50		TSP-100	
		LENGTH↓	GAP(%)↓	LENGTH↓	GAP(%)↓
CONCORDE	EXACT	5.69*	0.00	7.76*	0.00
2-OPT	HEURISTICS	5.86	2.95	8.03	3.54
AM	GREEDY	5.80	1.76	8.12	4.53
GCN	GREEDY	5.87	3.10	8.41	8.38
TRANSFORMER	GREEDY	5.71	0.31	7.88	1.42
POMO	GREEDY	5.73	0.64	7.84	1.07
SYM-NCO	GREEDY	-	-	7.84	0.94
DPDP	1k-IMPROVEMENTS	5.70	0.14	7.89	1.62
IMAGE DIFFUSION	GREEDY†	5.76	1.23	7.92	2.11
DIFUSCO	GREEDY†	<b>5.70</b>	<b>0.10</b>	<b>7.78</b>	<b>0.24</b>
DISCO (OURS)	GREEDY†	5.70	0.16	7.80	0.58
AM	1k×SAMPLING	5.73	0.52	7.94	2.26
GCN	2k×SAMPLING	5.70	0.01	7.87	1.39
TRANSFORMER	2k×SAMPLING	5.69	0.00	7.76	0.39
POMO	8×AUGMENT	5.69	0.03	7.77	0.14
SYM-NCO	100×SAMPLING	-	-	7.79	0.39
MDAM	50×SAMPLING	5.70	0.03	7.79	0.38
DPDP	100k-IMPROVEMENTS	5.70	0.00	7.77	0.00
DIFUSCO	16×SAMPLING	<b>5.69</b>	<b>-0.01</b>	<b>7.76</b>	<b>-0.01</b>
DISCO (OURS)	16×SAMPLING	<b>5.69</b>	<b>-0.01</b>	<b>7.76</b>	<b>0.03</b>



(a) Performance of baseline.



(b) Performance of DISCO.



(c) Runtime of DISCO.

Figure 5: The performance of both the baseline method DIFUSCO [80] (a) and DISCO (b) on TSP-50 instances with different denoising steps and sample number. Corresponding per-instance run-time (sec) of diffusion-based methods is depicted in (c). The negative performance gap arises because the Concorde solver, used for providing labels, only accepts integer coordinates as inputs, resulting in inaccurate non-optimal solutions due to rounding issues. For DISCO with a denoising step of 1, its variance  $\sigma$  tends to zero, as described by Eq. 8, yielding relatively more confident solutions and potentially better performance. However, this does not lead to performance improvement in response to actively sampling more times.

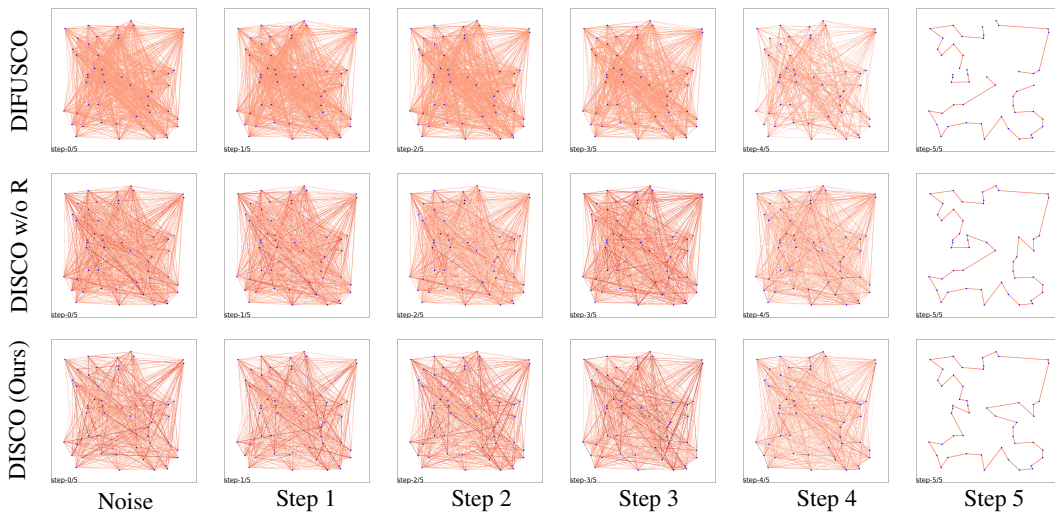


Figure 6: Denoising processes on TSP-50. Decoding the final heatmap with Greedy+2-opt yields tour lengths of **5.95** for DIFUSCO, **5.77** for DISCO without residues (w/o R), and **5.75** for DISCO.

## D Qualitative Results

### D.1 Denoising Processes on Large-Scale Instances

We illustrate the denoising processes of different diffusion methods on large-scale problems in Figure 7, using TSP-1000 as an example for clarity. The analytical denoising design and introduction of residues in DISCO ensure that high-quality solutions can be obtained with a few steps. In contrast, alternative methods generate solutions that frequently violate problem constraints, such as isolated nodes, non-closed tours, and inner loops.

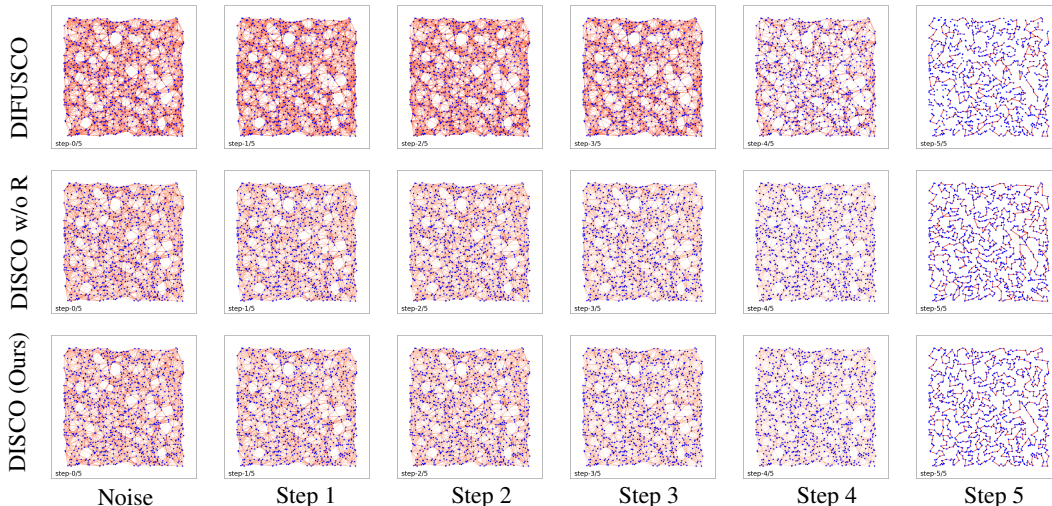


Figure 7: Denoising processes on TSP-1000. Decoding the final heatmap with Greedy+2-opt yields tour lengths of **27.69** for DIFUSCO, **26.33** for DISCO without residues (w/o R), and **25.35** for DISCO.

### D.2 Performance with Different Denoising Steps

Here, we demonstrate the final heatmaps  $\mathbf{x}_0$  generated by different denoising steps with different diffusion methods. The visualizations are summarized in Fig. 8, which still opt for TSP-1000 to ensure readability. The corresponding decoded tour lengths are annotated directly below each plot. It is evident that DISCO consistently produces high-quality solutions across various denoising steps. Particularly for time-sensitive scenarios requiring few denoising steps, DISCO maintains a significant advantage over the baselines.

## E Generalization to Real-World Instances

We evaluate DISCO on TSPLIB [73], a collection of real-world TSP scenarios, to assess its effectiveness in transferring knowledge from the synthetically generated data to the real world. We directly transfer the DISCO models trained on TSP-50 and TSP-100 to these real-world instances without any fine-tuning. Each instance strictly follows the evaluation protocol proposed by TSPLIB. The results are summarized in Tab. 6. We can observe that DISCO is the best performer in 28 out of 29 test cases. Notably, as a diffusion-based algorithm, DISCO’s solving speed is the fastest among all compared algorithms across all cases, further demonstrating its efficiency advantage and practicality. The test code and models for this part are provided in the Supplementary Material for reproducibility. We also provide visualizations of each solution generated by DISCO in Fig. 9.

## F Decoding Strategy

For offline problems [66; 70], all input data and all constraints are fully provided before solving the problems. The decision-makers can fully utilize all relevant information for comprehensive analysis and iteratively improve solution quality. Providing an initial solution by SL and further refining it

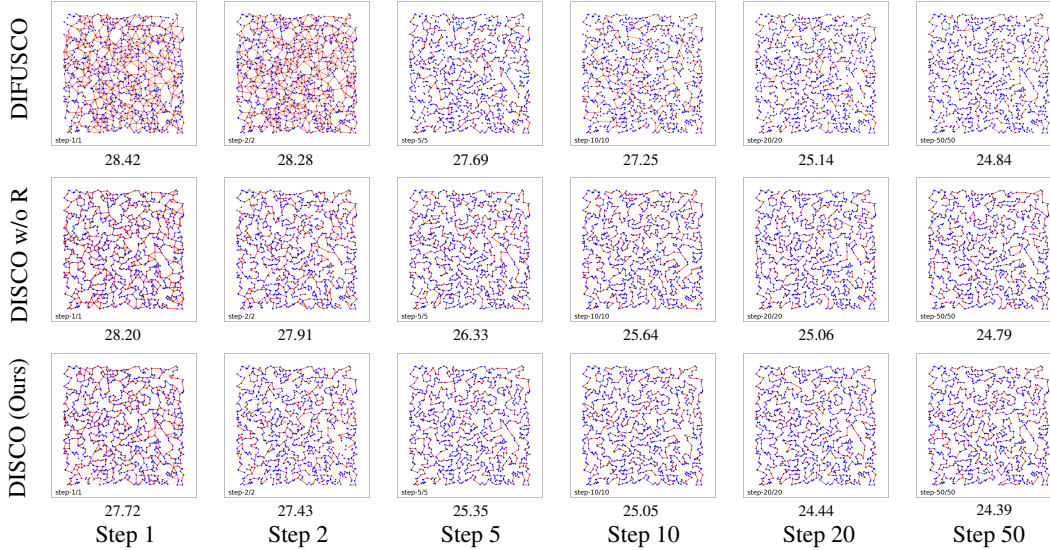


Figure 8: Generated heatmaps on TSP 1000-instances under different denoising steps, with the final decoded tour length captioned below. DISCO consistently produces higher-quality heatmaps that better satisfy the problem constraints, leading to better decoding results with the same number of denoising steps.

Table 6: TSPLIB performance. We indicate the training scales for DISCO/DIFUSCO in parentheses.

Method Instance	Kool et al. [52]		Joshi et al.[46]		Costa et al. [20]		Hudson et al. [43]		DIFUSCO (50)		DIFUSCO (100)		DISCO (50)		DISCO (100)	
	Time (s)	Gap (%)	Time (s)	Gap (%)	Time (s)	Gap (%)	Time (s)	Gap (%)	Time (s)	Gap (%)	Time (s)	Gap (%)	Time (s)	Gap (%)	Time (s)	Gap (%)
eil51	0.125	1.628	3.026	8.339	28.051	0.067	10.074	<b>0.000</b>	0.482	<b>0.000</b>	0.519	0.117	<b>0.049</b>	<b>0.000</b>	<b>0.049</b>	<b>0.000</b>
berlin52	0.129	4.169	3.068	33.225	31.874	0.449	10.103	0.142	0.527	<b>0.000</b>	0.526	<b>0.000</b>	<b>0.047</b>	<b>0.000</b>	0.048	<b>0.000</b>
st70	0.200	1.737	4.037	24.785	23.964	0.040	10.053	0.764	0.663	0.000	0.670	0.000	<b>0.062</b>	<b>-0.741</b>	0.064	<b>-0.741</b>
eil76	0.225	1.992	4.303	27.411	26.551	0.096	10.155	0.163	0.788	0.000	0.788	0.174	0.076	<b>-0.557</b>	<b>0.072</b>	<b>-0.557</b>
pr76	0.226	0.816	4.378	27.793	39.485	1.228	10.049	0.039	0.765	0.000	0.785	0.187	0.074	<b>-0.379</b>	<b>0.072</b>	<b>-0.379</b>
rat99	0.347	2.645	5.559	17.633	32.188	0.123	9.948	0.550	1.236	1.187	1.192	0.000	0.115	0.000	<b>0.103</b>	<b>-0.165</b>
kroA100	0.352	4.017	5.705	28.828	42.095	18.313	10.255	0.728	1.259	0.741	1.217	0.000	0.110	<b>-0.019</b>	<b>0.106</b>	<b>-0.019</b>
kroB100	0.352	5.142	5.712	34.686	35.137	1.119	10.317	0.147	1.252	0.648	1.235	0.742	0.116	<b>0.235</b>	<b>0.108</b>	0.262
kroC100	0.352	0.972	5.641	35.506	34.333	0.349	10.172	1.571	1.199	1.712	1.168	0.000	0.108	0.029	<b>0.103</b>	<b>-0.067</b>
kroD100	0.352	2.717	5.621	38.018	25.772	0.866	10.375	0.572	1.226	0.000	1.175	0.000	0.118	<b>-0.117</b>	<b>0.110</b>	<b>-0.117</b>
kroE100	0.352	1.470	5.650	26.589	34.475	1.832	10.270	1.216	1.208	0.274	1.197	0.274	0.114	0.168	<b>0.110</b>	<b>0.000</b>
rd100	0.352	3.407	5.737	50.432	28.963	0.003	10.125	0.459	1.191	0.000	1.172	0.000	0.101	<b>-0.733</b>	<b>0.097</b>	<b>-0.733</b>
eil101	0.359	2.994	5.790	26.701	23.842	0.387	10.276	0.201	1.222	0.576	1.215	0.000	0.114	<b>-0.318</b>	<b>0.107</b>	<b>-0.318</b>
lin105	0.380	1.739	5.938	34.902	39.517	1.867	10.330	0.606	1.321	0.000	1.280	0.000	0.124	<b>-0.306</b>	<b>0.107</b>	<b>-0.306</b>
pr107	0.391	3.933	5.964	80.564	29.039	0.898	9.977	0.439	1.381	0.228	1.378	0.415	0.148	<b>-0.199</b>	<b>0.144</b>	<b>-0.169</b>
pr124	0.499	3.677	7.059	70.146	29.570	10.322	10.360	0.755	1.803	0.925	1.782	0.494	<b>0.144</b>	<b>-0.198</b>	<b>0.144</b>	<b>0.151</b>
bier127	0.522	5.908	7.242	45.561	39.029	3.044	10.260	1.948	1.938	1.011	1.915	0.366	0.176	<b>-0.379</b>	<b>0.169</b>	<b>-1.026</b>
ch130	0.550	3.182	7.351	39.090	34.436	0.709	10.032	3.519	1.989	1.970	1.967	0.077	<b>0.153</b>	0.245	0.162	<b>-0.016</b>
pr136	0.585	5.064	7.727	58.673	31.056	0.000	10.379	3.387	2.184	2.490	2.142	0.000	<b>0.146</b>	0.069	0.180	<b>-0.342</b>
pr144	0.638	7.641	8.132	55.837	28.913	1.526	10.276	3.581	2.478	0.519	2.446	0.261	<b>0.159</b>	<b>-0.063</b>	0.186	<b>-0.063</b>
ch150	0.697	4.584	8.546	49.743	35.497	0.312	10.109	2.113	2.608	0.376	2.555	0.000	<b>0.169</b>	0.276	0.202	<b>-0.061</b>
kroA150	0.695	3.784	8.450	45.411	29.399	0.724	10.331	2.984	2.617	3.753	2.601	0.000	<b>0.174</b>	0.033	0.208	<b>-0.098</b>
kroB150	0.696	2.437	8.573	56.745	29.005	0.886	10.018	3.258	2.626	1.839	2.592	<b>0.067</b>	<b>0.176</b>	0.554	0.206	0.417
pr152	0.708	7.494	8.632	33.925	29.003	0.029	10.267	3.119	2.716	1.751	2.712	0.481	<b>0.183</b>	0.122	0.221	<b>-0.062</b>
u159	0.764	7.551	9.012	38.338	28.961	0.054	10.428	1.020	2.963	3.758	2.892	0.000	<b>0.184</b>	<b>-0.067</b>	0.196	<b>-0.067</b>
rat195	1.114	6.893	11.236	24.968	34.425	0.743	12.295	1.666	4.400	1.540	4.428	0.767	<b>0.266</b>	0.947	0.310	<b>0.560</b>
d198	1.153	373.020	11.519	62.351	30.864	0.522	12.596	4.772	4.615	4.832	4.153	3.337	<b>0.297</b>	0.330	0.375	<b>0.292</b>
kroA200	1.150	7.106	11.702	40.885	33.832	1.441	11.088	2.029	4.710	6.187	4.686	0.065	<b>0.301</b>	1.134	0.346	<b>-0.398</b>
kroB200	1.150	8.541	11.689	43.643	31.951	2.064	11.267	2.589	4.606	6.605	4.619	0.590	<b>0.301</b>	1.481	0.346	<b>0.065</b>
Mean	0.532	16.767	7.000	40.025	31.766	1.725	10.420	1.529	1.999	1.480	1.966	0.290	<b>0.149</b>	0.067	0.161	<b>-0.136</b>

by decoding strategies has become a common practice [22]. We introduce the following decoding strategies combined with DISCO, including greedy strategy [32], sampling strategy [52], 2-OPT decoding strategy [19], and MCTS [26].

**Greedy Strategy** We use a straightforward greedy strategy to decode solutions from heatmaps produced by probabilistic models. Specifically, we iteratively add the highest-scoring candidates among the remaining ones to the partial solution. We repeat this process until all relevant nodes/edges are incorporated. For diffusion-based methods, we sample the initial solution once with a single noise data  $\mathbf{x}_t$ . We set the denoising step as 1 for DISCO when executing this greedy strategy, allowing the variance  $\sigma$  to approach zero (as described in Eq. 8) to generate more confident solutions.

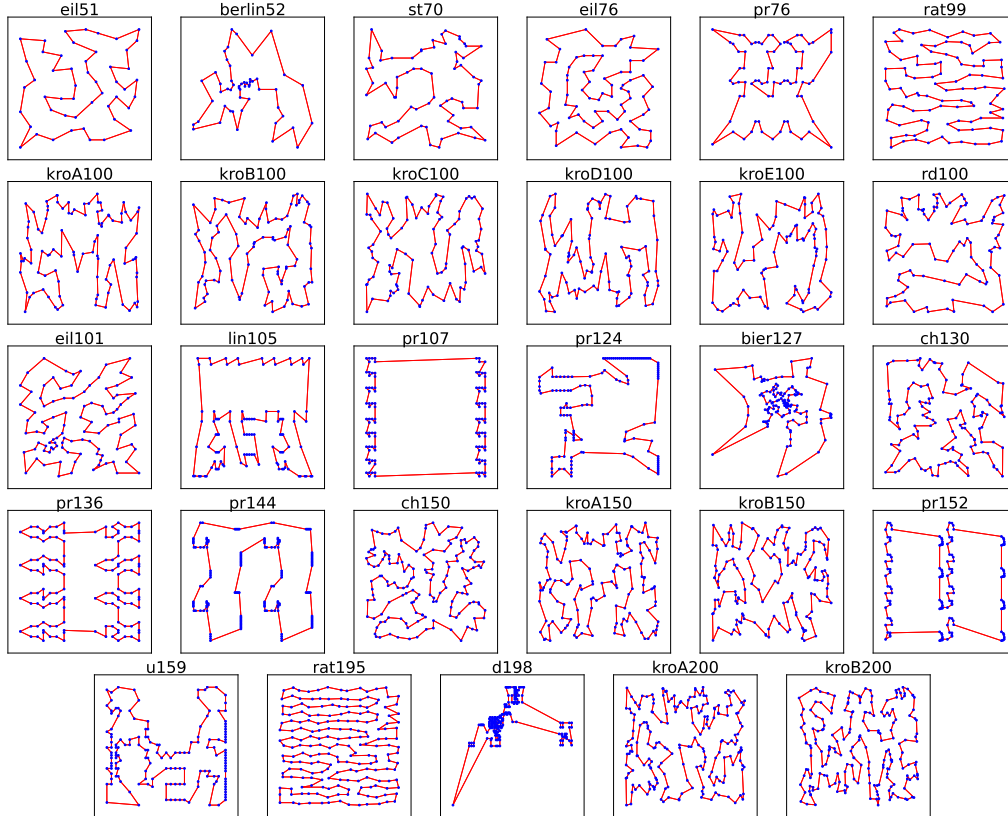


Figure 9: Visualization of DISCO’s generated solutions on TSPLIB instances.

**Sampling Strategy** Probabilistic solvers usually sample multiple solutions [52] through various means and execute the best one. Statistically, increasing the number of samples can enhance the breadth and depth while exploring the solution space, thereby increasing the probability of finding higher-quality solutions [96]. Following this logic, we generate multiple heatmaps from  $p_{\theta}(\mathbf{x}_0|s)$  with different noise data  $\mathbf{x}_i$ , and then apply the greedy decoding algorithm described above to each heatmap. For DISCO, we set the denoising step over 1 for heatmap generation, which allows the variance  $\sigma$  to be non-zero to enrich solution diversity, while introducing solution residues to constrain generations as high-quality as possible.

**2-opt Strategy** We also adopt a 2-opt decoding strategy [2] to refine the greedy solutions of TSP tasks. Specifically, we iteratively swap two edges in the current solution to reduce the total length of the tour. We repeat this process until no further improvement can be made. We follow Graikos et al. [32] and use this Greedy+2-opt decoding strategy as the default.

**Monte Carlo Tree Search** Building on the work of Fu et al., [26], we enhance TSP solutions with Monte Carlo tree search (MCTS) [75; 77]. We employ  $k$ -opt transformation actions guided by heatmaps produced by the parameterized model to refine current solutions. MCTS executes simulation, selection, and back-propagation phases until the sampling pool yields no further improvements. Although MCTS typically exhibits stronger performance than other decoding methods, its iterative solution updating approach also tends to incur higher computational costs. We recommend that our users select the appropriate decoding strategy based on their customized needs.

We conduct DISCO combined with all these strategies on TSP instances to demonstrate its robustness. Following instructions from [9], we only conduct greedy strategy and sampling strategy on MIS instances to fairly compare the capabilities of different parameterized solvers.

## G Implementation Details

**Training Setting** We adopt anisotropic GNNs [85] as the backbone of our DISCO model. Anisotropic GNNs can produce embeddings for both nodes and edges, which exactly match the

CO problems most of which can be formulated as graph problems. Specifically, we input the noisy solution  $\mathbf{x}_t$ , the node and edge features of  $\mathbf{X}_d$ , and the time  $t$  into the anisotropic GNN with parameter  $\theta$ , predicting the parameterized residue  $\mathbf{x}_{res}^\theta$  and noise  $\epsilon^\theta$  simultaneously. We adopt a linear schedule [40] to gradually reduce the noise during the model’s generation process.

Following Sun and Yang [80], we implement sparsification in large-scale graph problems to diminish computational complexity. We constrain each node to maintain only  $k$  edges connecting to its closest neighbors. Specifically, we limit  $k$  to 50 for TSP-500 and increase it to 100 for TSP-1000/10000. We also directly transfer the trained models to the same graphs with different sparsifications without fine-tuning, the generalization results are summarized in Tab. 7. We can observe that DISCO performs consistently stable while the sparsification changes, indicating its robustness.

Table 7: Evaluation results on different sparsification  $k$ . The symbol  $\circ$  indicates the sparsification used for training, while the other lines are directly generalized without fine-tuning.

ALGORITHM	TYPE	$k$	TSP-500		TSP-1000		TSP-10000	
			LENGTH $\downarrow$	TIME $\downarrow$	LENGTH $\downarrow$	TIME $\downarrow$	LENGTH $\downarrow$	TIME $\downarrow$
DISCO	SL+G $\dagger$ +2-OPT	50	16.86 $^\circ$	0.25m	23.70	0.78m	73.85	24.80m
DISCO	SL+G $\dagger$ +2-OPT	100	16.99	0.50m	23.65 $^\circ$	1.12m	73.85 $^\circ$	25.12m
DISCO	SL+S+2-OPT	50	16.73 $^\circ$	3.88m	23.60	8.93m	73.82	1.48h
DISCO	SL+S+2-OPT	100	16.85	6.68m	23.56 $^\circ$	9.62m	73.81 $^\circ$	1.60h
DISCO	SL+MCTS	50	16.63 $^\circ$	6.99m	23.62	14.25m	73.58	42.03m
DISCO	SL+MCTS	100	16.70	7.07m	23.42 $^\circ$	15.82m	73.56 $^\circ$	42.35m

For the TSP-50 and TSP-100 instances, we utilize 1502000 random instances, training with batch sizes of 256 and 128 respectively. For TSP-500 and TSP-1000 challenges, we train DISCO with instances of 128000 and 64000 and batch size of 32. For TSP-10000, the model is trained using 6,400 instances with a batch size of 4. Align with DIFUSCO [80], we incorporate curriculum learning approach[6] and begin the training process for TSP-500/1000 from the TSP-100 checkpoint, and for TSP-10000 from the TSP-500 checkpoint. We label the training instances for TSP-50/100 using the Concorde solver. For TSP-500/1000/10000, we label training instances using the LKH-3 heuristic solver [34] with 1000 trials.

For the MIS instances, we use the training split of 49500 examples from SATLIB [38], training with a batch size of 64. For Erdős-Rényi [25] graph sets, we use 60000 random instances from the ER-[700-800] variant and train DISCO with a batch size of 16. The training instances of labeled by the KaMIS heuristic solver [54].

**Evaluation Details** We conduct extensive evaluations on both TSP and MIS instances to demonstrate the superiority of our DISCO model. We keep our experimental settings consistent with previous literature [71; 80]. For TSP-500 and TSP-1000, we take 128 instances as the test set, while for TSP-10000, we use 16 instances. For small-scale TSP instances, i.e., TSP-50 and TSP-100, we evaluate on 1280 instances. For MIS instances, we evaluate on 500 instances on SATLIB [38] and 128 instances on ER-[700-800] [25] graph sets.

Given that diffusion models are capable of generating diverse samples from their distribution, for each experiment, we evaluate DISCO 5 times with different random seeds and report the averaged results. We summarize the experimental results on large-scale TSP instances in Tab. 8. We also provide the standard deviation (Std) of these repeated evaluations to demonstrate the stability of our method. Our algorithm consistently demonstrates low variance and little fluctuations in performance, indicating its robustness across different runs.

Table 8: Statistical analysis of repeated evaluations on large-scale TSP problems. MS denotes our multi-modality inspired graph search method, where each search samples 50 solution trials.

ALGORITHM	TYPE	TSP-500			TSP-1000			TSP-10000		
		LENGTH $\downarrow$	STD $\downarrow$	TIME $\downarrow$	LENGTH $\downarrow$	STD $\downarrow$	TIME $\downarrow$	LENGTH $\downarrow$	STD $\downarrow$	TIME $\downarrow$
DISCO	SL+G $\dagger$ +2-OPT	16.862 $\pm$ 0.008	$4.81 \times 10^{-2}$	0.25m	23.653 $\pm$ 0.005	$2.92 \times 10^{-3}$	1.12m	73.851 $\pm$ 0.035	$3.00 \times 10^{-2}$	25.12m
DISCO	SL+S+2-OPT	16.733 $\pm$ 0.002	$1.14 \times 10^{-3}$	3.88m	23.651 $\pm$ 0.007	$5.77 \times 10^{-3}$	9.62m	73.811 $\pm$ 0.031	$3.51 \times 10^{-2}$	1.60h
DISCO	SL+MCTS	16.632 $\pm$ 0.004	$2.68 \times 10^{-3}$	6.99m	23.419 $\pm$ 0.004	$2.91 \times 10^{-3}$	15.82m	73.562 $\pm$ 0.029	$3.27 \times 10^{-2}$	42.35m
DISCO + MS	SL+G $\dagger$ +2-OPT	16.789 $\pm$ 0.005	$3.49 \times 10^{-3}$	11.67m	23.614 $\pm$ 0.003	$2.51 \times 10^{-3}$	28.83m	74.240 $\pm$ 0.034	$3.21 \times 10^{-2}$	1.82h